ResearchOnline@JCU



This is the author-created version of the following work:

Prajapati, Megha, Singh, Vinamrita, Jacob, Mohan V., and Ravi Kant, Chhaya (2023) *Recent advancement in metal-organic frameworks and composites for high-performance supercapatteries*. Renewable and Sustainable Energy Reviews, 183.

Access to this file is available from:

https://researchonline.jcu.edu.au/79465/

Please refer to the original source for the final version of this work:

https://doi.org/10.1016/j.rser.2023.113509

Recent Advancement in Metal-Organic Frameworks and Composites for 1

- **High-performance Supercapatteries.** 2
- Megha Prajapati^{1,3}, Vinamrita Singh², Mohan V. Jacob³, Chhaya Ravi Kant^{1*} 3
- ¹Department of Applied Sciences and Humanities, Indira Gandhi Delhi Technical University 4
- for Women, Delhi-110006, INDIA 5
- ²Department of Physics, Netaji Subhas University of Technology, East Campus, Delhi-6
- 110031, INDIA 7
- 8 ³Electronics Materials Lab, College of Science and Engineering, James Cook University,
- 9 Townsville, QLD 4811, Australia
- Corresponding Author E-mail * chhayaravikant@igdtuw.ac.in 10

11 12

Abstract:

13 14

15

16 17

18

19

20

21

22

23

24

25

26

27

28 29 High-performance electrochemical energy storage devices concurrently require enhanced energy density, power density, and long lifespan, which has led to the emergence of supercapattery technology. Supercapatteries are on a rapid development path with the emergence of suitable electrode materials and befitting device architecture that integrates high energy density of batteries with the high-power density and cyclability of supercapacitors in a single device. Transition metal compounds have achieved a benchmark in supercapatteries, but these compounds face challenges in controllable structure and porosity to achieve better electrochemical performance. Multifunctional metal-organic frameworks (MOFs) appear as the next-generation material and have fascinated immense consideration in supercapattery applications. Their outstanding properties like high specific surface area with controllable pore structure and architectural tunability has resulted in the advancement of active electrode materials for supercapatteries. This review critically examines the current progress in transition metal compound based electrode materials and advancement of MOF-derived structures and their composites for supercapattery applications. This review article highlights the potential in MOF-based supercapatteries that provides a blueprint for next-generation, high performance electrochemical energy storage systems.

30 31

- Keywords: Metal-organic frameworks, Supercapattery, Power density, Energy density,
- Transition metal compounds, Electrochemical energy storage 32

33 34

Contents

35 36 37

- 39 2. Charge storage mechanism in electrochemical energy storage devices......4
- 40 2.1. Batteries
- 2.2. Supercapacitors 41

1		2.3. Supercapattery
2		
3	3.	Supercapatteries based on transition metal compounds8
4	4.	Supercapatteries based on metal-organic frameworks
5	4.1. Sy	nthesis and characteristics of MOFs
6		4.2. MOF derivatives based supercapattery
7		4.3. MOF composites based supercapattery
8	5.	Conclusion and future perspective
9		

1. INTRODUCTION

Electrochemical energy storage (EES) devices are crucial for storing and delivering energy at every scale while eliminating the reliance on renewable sources such as tidal energy, solar energy, wind energy, etc. [1]. EES devices can hold large amounts of energy, deliver high power, have a long lifespan, and are viably affordable. EES devices like rechargeable batteries [2]–[4] possess adequately high energy densities, whereas supercapacitors [5]–[8] own high power densities and extensive cycle lifespans. Despite a lot of advancement in both these technologies, they cannot embark on the desirable commercialization for a wide range of applications. Rechargeable batteries suffer from low power density, less cycle life, and joule heating [9]. On the other hand, supercapacitors suffer from low energy density and inadequate potential [6]. To resolve this, ongoing research is focused on combining the merits of rechargeable batteries and supercapacitors into a single device known as supercapattery [10]. The Ragone plot given in Figure 1 displays the difference between various EES devices based on their energy density and power density. The plot also demonstrates that supercapattery bridges the gap between the batteries and the supercapacitors as summarised in Table 1.

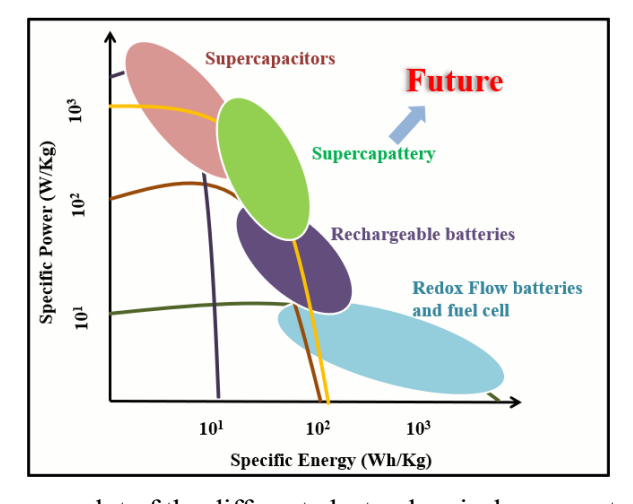


Figure 1. Ragone plot of the different electrochemical energy storage devices

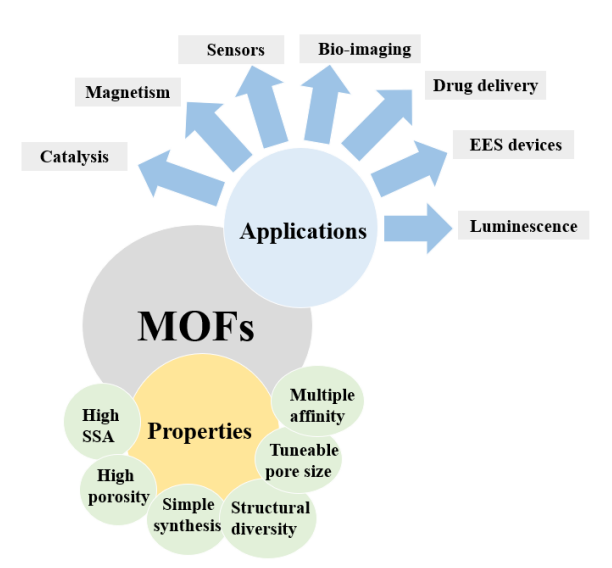
Performance of EES devices prominently relies on the choice of electrode materials; therefore, majority of the research is focused on integrated electrode architectures built with nanomaterials available in numerous chemical configurations and morphologies. Among them, metal-organic frameworks, abbreviated as MOFs, are currently receiving much attention in the pursuit of the best electrode materials for potential applications in rechargeable batteries [11], supercapacitors [12], and supercapattery [13]. MOFs have unique morphologies with isoreticular structures that exhibit incredible properties like high and uniform porosity, large pore volume, high surface area ($\approx 2000-8000 \text{ m}^2/\text{g}$), structural uniformity, tuneable functionality,

and structural diversity achieved with simple synthesis methods. They are formed by combining metal ions (such as Zn²⁺, Cu²⁺, Ni²⁺, Al³⁺, Cr³⁺, Fe³⁺, Zr⁴⁺, etc.) with multidentate organic linkers via coordination bonding. The organic linkers range from the vast family of carboxylic acids, bipyridine, benzoic acids, phenylene, and terephthalic acids. MOFs can be produced in innumerable combinations for targeted purpose due to the vast range of available metal species and organic linkers. MOF structures can be made in one dimension (1-D), two dimensions (2-D), or three dimensions (3-D), depending upon the organic and inorganic structural units [14]–[16].

Table 1. Comparison of different electrochemical energy storage devices

	Capacitors [17]	Supercapatteries	Batteries	Supercapacitors [17]
Energy density	< 0.1 Wh/kg	10-100 Wh/kg [18]–[22]	120240 Wh/kg [23]	1-10 Wh/kg
Power density	>>10,000 W/Kg	100-1000 W/kg [24]–[28]	1-3 kW/kg (Li-ion battery) [23]	500-10 kW/kg
Cycle life	Infinite	> 10,000 [29]	About 1000 [17]	> 500,000
Charging time	10 ⁻⁶ to 10 ⁻³ sec		1-5 h [17]	Sec to mins
Discharging time	10 ⁻⁶ to 10 ⁻³ sec		0.3 to 3 h [17]	Sec to mins

A variety of synthetic techniques exist to synthesize MOFs by combining metal ions with organic linkers using high boiling point solvents such as N, N-dialkyl formamides or even deionized water. These techniques include botconventional synthesis methods like heating in the oven and also specific ones such as microwave [30], electrochemical [31], ultrasonic [32], and mechanochemical processing. The obtained MOF structures possess distinctive structural properties which makes them extensively useful in a number of applications such as gas storage and separation [33]–[35], MOF magnets [36]–[41], catalysis [42], [43], sensors [44]–[46], drug delivery [47]–[49], bioimaging [37]-[38], luminescence [52], and electrochemical energy storage [53]–[58] as illustrated in Figure 2.



MOF-based electrodes in electrochemical systems provide inherent redox-active sites and improved storage capacity. Recent advancements in the MOFs include deriving nanoporous carbon [59]–[61], metal oxide/hydroxides nanostructures, and nanocomposites that make them applicable as cathode, anode, matrix, and precursors in EES devices [5]. The relevance of MOFs as potential electrode material has led to a new area of research with efforts to amalgamate the charge storage mechanisms prevalent in supercapacitors and rechargeable batteries towards a hybridized supercapattery mechanism. In this review paper, the current research progress, challenges, and scope for future work in the emerging field of supercapatteries is outlined with the aim to understand the working and charge storage mechanism to achieve significantly high energy density and power density for idealistic EES devices.

2. Charge storage mechanism in electrochemical energy storage devices

The term supercapattery is designed with the word "supercap" (from the term supercapacitor) and "attery" (from the term battery) because of the involvement of both types of charge storage technologies. It is essential to understand the charge storage mechanism in batteries and supercapacitors to comprehend the working mechanism of supercapatteries.

2.1. Batteries

Rechargeable batteries are composed of two electrodes, cathode and anode, and an electrolytic solution (Figure 3a). The rechargeable batteries store energy electrochemically within the bulk of the electrodes, which act as host materials for the electrolyte ions. The electrode materials are chosen in such a way that the electrolyte ions can intercalate/deintercalate during the charging and discharging processes. During the charging cycle, the positive electrolyte ions are deintercalated (extracted) from the cathode and intercalated (inserted) into the anode. The reverse process occurs during the discharging cycle where the positive ions transport from the anode to the cathode. This charge transfer mechanism involves Faradic reverse oxidation and reduction reactions that occur between the electrodes when a battery is connected to an external electric load. Thus, energy in batteries is stored through reversible redox reactions. The Faradic charge storage mechanism is evident from the peaks in cyclic voltammetry (CV) and asymmetric curve in galvanostatic chargedischarge (GCD) measurements as shown in Figure 3b,c. Transition metals and their derivatives of oxides [62]-[65], hydroxides, phosphides [66]-[68], nitrides [69][70], and different polymers [71] are utilized as electrode material in batteries. The most prominent batteries in the current scenario are Li-ion batteries [2][72], Na-ion batteries [73][74], and Limetal batteries [75]-[77]. Li-ion batteries are environmentally friendly and have tremendous energy density (LiS 2600 Wh/kg, LiO 3505 Wh/kg). In addition, Li-metal batteries (Li-cobalt oxide, Li-phosphate, etc.) are also gaining immense interest because of their higher energy capacity of 3860 mAh/kg and low-cost electrolyte additives. Thus, batteries give tremendous results when we consider the energy density parameter but power density and cyclability are still very low [78]. Supercapacitors resolve this issue to great extent and are considered to bridge the gaps between batteries and capacitors [17].

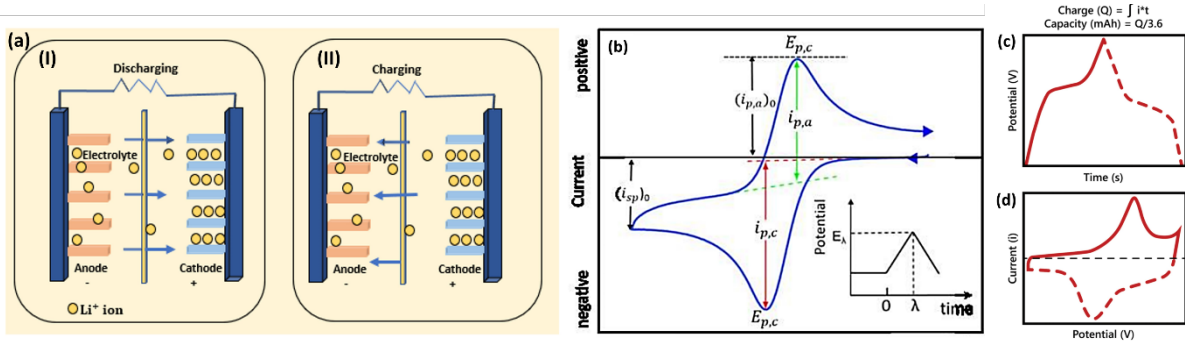


Figure 3. Schematic diagram of battery: (a). charge storage mechanism of battery; (I) discharging; (II) charging; (b)(d). schematic cyclic voltammograms; (c). galvanostatic charge-discharge curve. (b). Reproduced with permission copyright 2017, John Wiley and Sons; [79] (c,d). Reproduced with permission copyright 2017, John Wiley and Sons [80]

2.2. Supercapacitors

Supercapacitors (SCs), also recognised as ultracapacitors, are composed of two electrodes with high surface area and separated by a thin cellulose separator dipped in an electrolytic solution (Figure 4a). SCs offer remarkable capacitance and energy density in comparison to conventional capacitors [17]. Based on the technique for storing charges, SCs are commonly categorized as electric double layer capacitor (EDLC) and pseudocapacitors (Figure 4a). EDLC SCs are chiefly governed by the charge accumulation on the electrode-electrolyte interface, which is non-faradaic and electrostatic in nature. There is no chemical or physical transformation inside the electrode surface resulting in the high cyclability of these devices [61]. The CV curves of EDLC devices are rectangular in shape, and ideally, GCD curves (Figure 4b) are symmetric. The most popular materials for EDLC supercapacitors are carbon-based materials [81]–[83].

Another charge storage mechanism involving interface-confined redox reactions or intercalation/deintercalation of electrolytic ions, i.e., pseudocapacitance, results in higher specific capacitance and energy density than EDLC SCs but is still lower than rechargeable batteries. The CV and GCD graphs of pseudocapacitors (Figure 4c,d,e), clearly show distinguished peaks of redox reactions and asymmetric charging-discharging behaviour. The materials employed in pseudocapacitors are composites of conducting polymers (polyaniline (PANI), polythiophene, polypyrrole (Ppy), polyacetylene, etc.) and transition metal oxides (RuO₂, MnO₂, Co₃O₄, V₂O₅, Fe₃O₄, etc.) [84]–[86]. Pseudocapacitors suffer from several drawbacks including low power density and are more likely to alter their density during charging and discharging cycles, which reduces their cyclability [7][60].

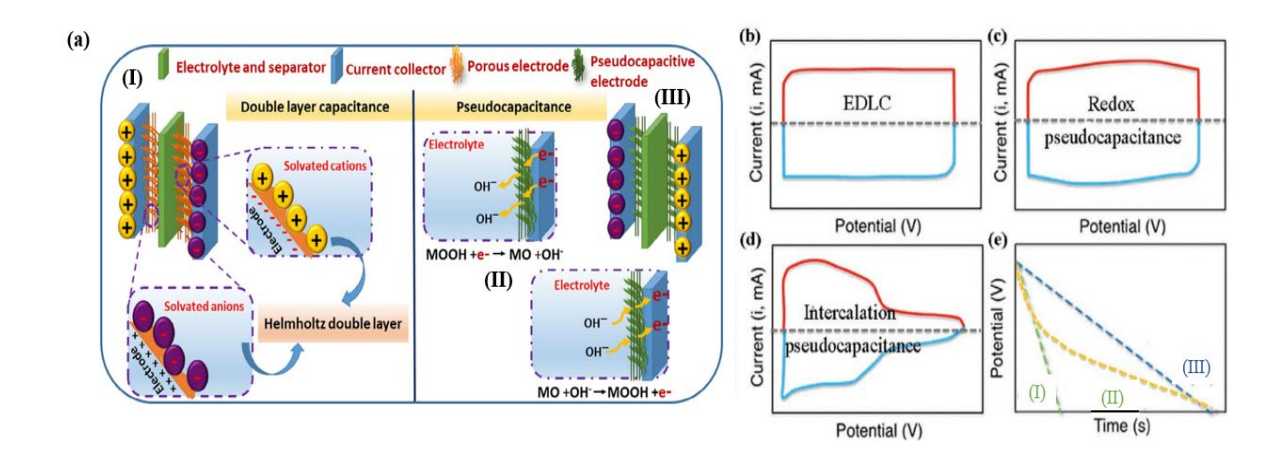


Figure 4. (a). Different energy storage mechanisms in supercapacitors: (I). carbon particles; (II). Redox pseudocapacitance; (III). Intercalation pseudocapacitance [87]. Schematic CV curves of: (b). EDLC; (c). redox pseudocapacitance; (d). intercalation pseudocapacitance; and (e). comparison of galvanostatic discharge plots for different energy storage mechanisms in supercapacitors; (a). Reproduced with permission copyright 2017, John Wiley and Sons; (b-e). Reproduced with permission copyright 2018, American Chemical Society [88]

2.3. Supercapattery

Combining two different technologies, i.e., rechargeable batteries and supercapacitors gave an upsurge to a newly established technology termed "supercapattery" as shown in Figure 5. Supercapattery provides an energy storage mechanism displaying high energy density and power density as well as fast charging and discharging capabilities [89]. The basic structure of asupercapattery device is similar to the supercapacitor comprising two electrodes separated by an electrolytic solution and a separator. A supercapattery can be described via Dunn's power law formula in accordance with the equation given below:

$$i = kv^b$$
.....(1)
 $ln(i) = ln(k) + b ln(v)$(2)

Where i defines current density (A/g), v (mV/s) defines scan rate, and b and k are adjustable parameters. b is an important parameter whose value changes in accordance with the charge storage mechanism. Ideally, b is found to be 1 for EDLC SCs and capacitors, where charge storage is mainly through the electrostatic mechanism. In the case of batteries value of b is found to be 0.5, as charge storage is through a faradic mechanism (oxidation-reduction) and for supercapattery device fitting value of b is in the region of 0.5–0.8, which is midway between battery and supercapacitors. Supercapattery is likely to attain high performance and long cycle life as it utilizes both capacitive and battery-grade material [90].

Generally, the hybridisation of two types of charge storage mechanisms can be carried out either at the device level or at the electrode material level. In the former case, battery-grade materials are combined with capacitive electrode materials to make a composite [91][92]. In the latter case, the individual electrode of battery type and capacitive electrode are combined to form the device. Carbon materials like graphene oxide, reduced graphene oxide, activated carbon (AC), carbon nanotubes (CNT), and fullerenes possessing high specific surface area (500-2500 m²/g) are utilized as capacitive electrode materials [92][93].

While combining a battery-grade negative electrode and a capacitive positive electrode in one cell, the following charge conservation equation is obeyed [21]:

$$Q^{-} = m^{-}C^{sp-}\Delta U^{-} = m^{+}C^{sp+}\Delta U^{+} = Q^{+}....(3)$$

where m is the effective mass of the electrode. C^{sp} is specific capacitance, Q is the total charge stored on the respective electrode and ΔU is the potential range. The "-" and "+" superscripts are used for negative and positive electrodes, respectively. Here, Q = nF/m where F represents Faraday constant, and the mass ratios of the electrodes are:

$$\frac{m^+}{m^-} = \frac{C^{sp-}\Delta U^-}{C^{sp+}\Delta U^+} \dots (4)$$

The architecture of the electrodes is engineered according to equation (4). In case of hybrid supercapacitors, the two electrodes have different capacitances and/or different operating voltages. This leads to unbalanced charge storage and the excess charges on one electrode do not contribute to the total capacitance. To account for this difference and achieve optimum cell voltage, the active mass of the electrodes is adjusted based on equation (4) leading to mass balancing and higher energy density.

In a nutshell, there are three charge storage techniques involved in supercapatteries. The first technique uses EDLC, based on porous materials like carbon nanotubes, activated carbon, and graphene to store charge reversibly on the electrode surface. The second mechanism is a non-capacitive Faradaic process, which is employed in rechargeable lead-acid batteries and

zinc-manganese dioxide batteries. The transfer of localised valence electrons is described by the Nernst equation. The third mechanism uses pseudocapacitance, also known as the capacitive Faradaic process, and describes the transport of delocalized valence electrons. This mechanism is usually seen in transition metal oxides (TMOs), which include RuO₂, SnO₂, MnO₂, etc. and electrically conducting polymers (ECPs) like poly (3,4-ethylene dioxythiophene) (PEDOT), polyaniline (PANI), and polypyrrole. Here, all three methods of charge storage can be used for electrode materials in supercapatteries [94][29].

The different materials utilized in supercapattery applications for battery type electrodes are transition metal phosphates, sulphides, oxides/hydroxides conducting polymers, and MOFs that are summarised in Table 2-6.

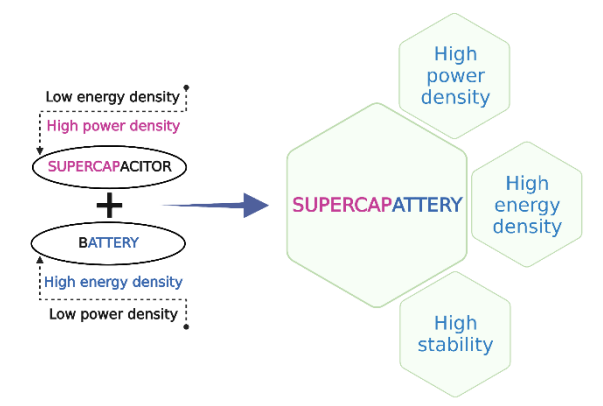
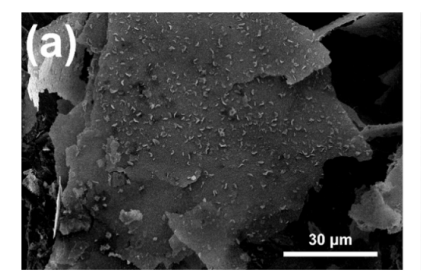


Figure 5. Integration of battery and supercapacitor technology

3. Supercapatteries based on transition metal compounds

 The performance of supercapattery majorly relies on the electrode material, therefore, scientists and researchers have worked out on integrating different electrode architectures. Among them, a number of transition metal-based oxides/phosphides/sulphides are selected for a hybrid system under the chase to search for the best available metal resources, tenable electrode materials, and low cost materials leading to increased volumetric and gravimetric energy densities [95]. A brief study on transition metal-based oxide/phosphide/sulphide materials for supercapatteries is summarised below.

Metal oxides offer abundant active sites, high electrochemical stability, and different oxidation states that result in substantial advancement in the electrochemical properties of supercapattery devices. The oxygen vacancies in metal oxides serve as shallow donors and as electrochemically active sites, which together boost the material's overall utilisation rate. Presently, metal oxides including cobalt oxide, molybdenum dioxide, manganese oxide, nickel oxide, and strontium oxide are extensively employed as an electrode material for supercapatteries [18], [96]–[98]. Along with mono metal oxides, multi-metal oxides are also largely employed in supercapattery applications for enhancing the redox-active sites for electrochemical properties. Multi-metal oxides offer multiple oxidation states and the metal species synergize to deliver more Faradaic active sites with an increase in conductivity of electroactive material [19], [20], [91], [93], [99], [100]. Table 2 summarizes the performance of metal oxide-based supercapatteries. Liang et al. [93] synthesized and studied 2D Mn_{0.4}Ni_{0.1}Co-OA thin sheets. SEM images (Figure 6a,b,c) of Mn_{0.4}Ni_{0.1}Co-OA demonstrates a honeycomb structured 3D network made of disordered interwoven 2D nanosheets with numerous pore walls and open channels that allow easy access to the electrolyte and boost the material's active surface area.



3

4

5 6

7 8

9

10

11 12

13

14

15

16

17

18

19

20

21 22

23

24

25

26

27

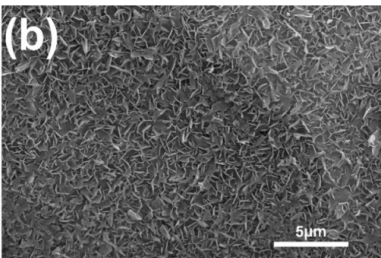
28 29

30

31 32

33 34

35



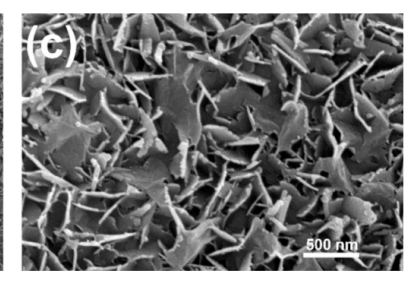


Figure 6. SEM images of Mn_{0.4}Ni_{0.1}Co-OA thin sheets at different magnifications: (a). 30 μm; (b). 5 μm; (c). 500 nm; (a-c). Reproduced with permission copyright 2021, Elsevier [93]

Mn_{0.4}Ni_{0.1}Co-OA was investigated as a positive electrode of the supercapattery and AC was used for the negative electrode. These electrodes provided an energy density, E_s, of 32.2 Wh/kg and power density, Ps, of 770.2 W/kg, respectively. The constructed device showed high stability and projected a coulombic efficiency of 88.1% over 15,000 cycles [93]. Further, defects in metal oxides play an additive role in enhancing the energy densities and power densities of the devices. Dominant oxygen deficiencies cause in situ crystal defects at various lattice sites, which is typically accomplished by the elimination of terminal oxygen using reducing reagents (NaBH₄, LiAlH₄) and high-temperature annealing [101] that increases the conductivity and open new paths for electron transfer in electroactive materials [102], [103]. Gurusamy et al. [97] reported the study of 2D MoO_{3-x} (x indicates oxygen vacancy) as an electrode material. Oxygen deficiencies and defects in 2D MoO_{3-x} (x indicates oxygen vacancy) nanoplates led to an improvement in the electrochemical properties of the supercapattery. It was observed from the HR-TEM images that the 2D MoO_{3-x} nanoplates consisted of regions having screw dislocations, amorphous boundaries, grain boundaries, and twin grain boundaries. Figure 7a depicts the screw dislocation as compared to a perfect crystal in which vacancies are simultaneously created. These vacancies are used up for energy storage by allowing the electrolyte ions to quickly adsorb/desorb on the surface of the electrodes. Fig. 7b shows the diffusion pathways of the electrons across grain boundaries, while Fig. 7c depicts the diffusion pathways along amorphous boundaries. The CV graphs of 2-D MoO_{3-x} in a threeelectrode arrangement depict redox peaks that represent the behaviour of a battery. With a power density of 11.6 kW/kg (1 A/g) and a cell voltage up to 1.6 V, MoO_{3-x} demonstrates an excellent energy density of 129.6 Wh/kg due to the absence of oxygen, which acts as highly reactive sites for the adsorption of electrolyte ions. Even after 10,000 GCD cycles the device kept a phenomenal capacitance retention of 98.6% [97].

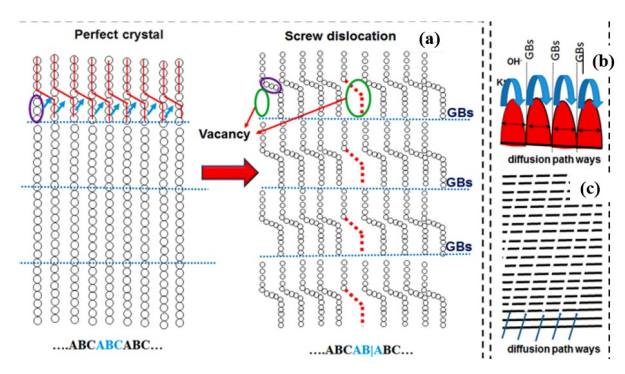


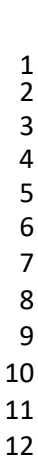
Figure 7. Screw dislocation: (a). grain boundary; diffusion pathways of (b). grain boundary and (c) amorphous boundary; (a-c). Reproduced with permission copyright 2020, Elsevier [97]

Further, the integration of mono metal and multi-metal oxides with conducting materials like conducting polymers, metal nanoparticles (Ag, Au, etc.), and carbonaceous materials (rGO,

CNT, etc.) [21][103][104] [105] are beneficial for improving the mechanical stability and ion diffusion rate due to increased conductivity for enhanced electrochemical properties [19][103]. Iqbal et al. [19] synthesized SrO@PANI composite through physical blending. The composites' specific conductivity and electrochemical performance were improved by the interphase region between PANI and SrO. Initially, the samples were analysed in a three-electrode configuration at varying scan rates ranging between 0 and 0.6 V. The CV curves showed the redox peaks which depict the behaviour of a battery. Conducting matrix of PANI offers an electroactive pathway for ion diffusion and boosts the electrochemical reversibility as evident from the CV curve that have a sharp horizontal shift with incorporation of PANI in SrO. GCD curve showed an increase in the discharging time due to large surface area offered to electrolytic ions by SrO@PANI. For supercapattery analysis, the SrO@PANI is employed as the anode and AC as the positive electrode. The potential window of the assembly SrO@PANI//AC is improved (1.6 V) as compared to SrO@PANI (0.6 V) and AC electrode (1 V). Furthermore, the device shows cyclic stability of 114% after 3000 charge-discharge cycles [19].

 Metal oxides exhibit a high surface-to-volume ratio, yet in their pristine form they coalesce leading to reduction of electroactive sites thereby deteriorating specific capacity [106]. Although substantial work is done on metal oxides-based electrodes, the commercial applicability of these materials is obstructed by poor electrical conductivity and low electrochemical cycling stability. Further, phosphides-based materials have been used for supercapatteries due to their good electrical conductivity and fast ion transport mechanism. Metal phosphides are expected to show metallic and semiconducting behaviour because of the abundant strong metal-phosphorus bonds and metal-metal bonds, that give rise to high electrical conductivity with significant chemical stability [107]. Due to their rapid ion transport mechanism, metal phosphates such as cobalt, manganese, and nickel phosphate and their multimetal phosphates can be ideal electrode materials for supercapatteries [108]–[113]. Table 3 summarizes the performance of metal phosphate-based supercapatteries.

Shao et al. [114] reported cobalt phosphate nanoflakes grown in situ on Ni foam using the hydrothermal technique and employed as supercapattery electrode with AC. The samples were tested in three electrodes configuration. Battery-like behaviour was confirmed by the quasi-reversible plots with distinct potential plateaus in GCD. It was found that 3D networks of thin nanoflakes of cobalt phosphate project a large contact area with lots of nano/microscale gaps. This favored fast charge transport and deeper electrolyte access to the interior surfaces of the electrode yielding specific capacitance of 1990 F/g. Further, the high thermal stability of the supercapattery was demonstrated by operating it as a pacemaker power source at average human body temperature (25–45 °C) (Figure 8).



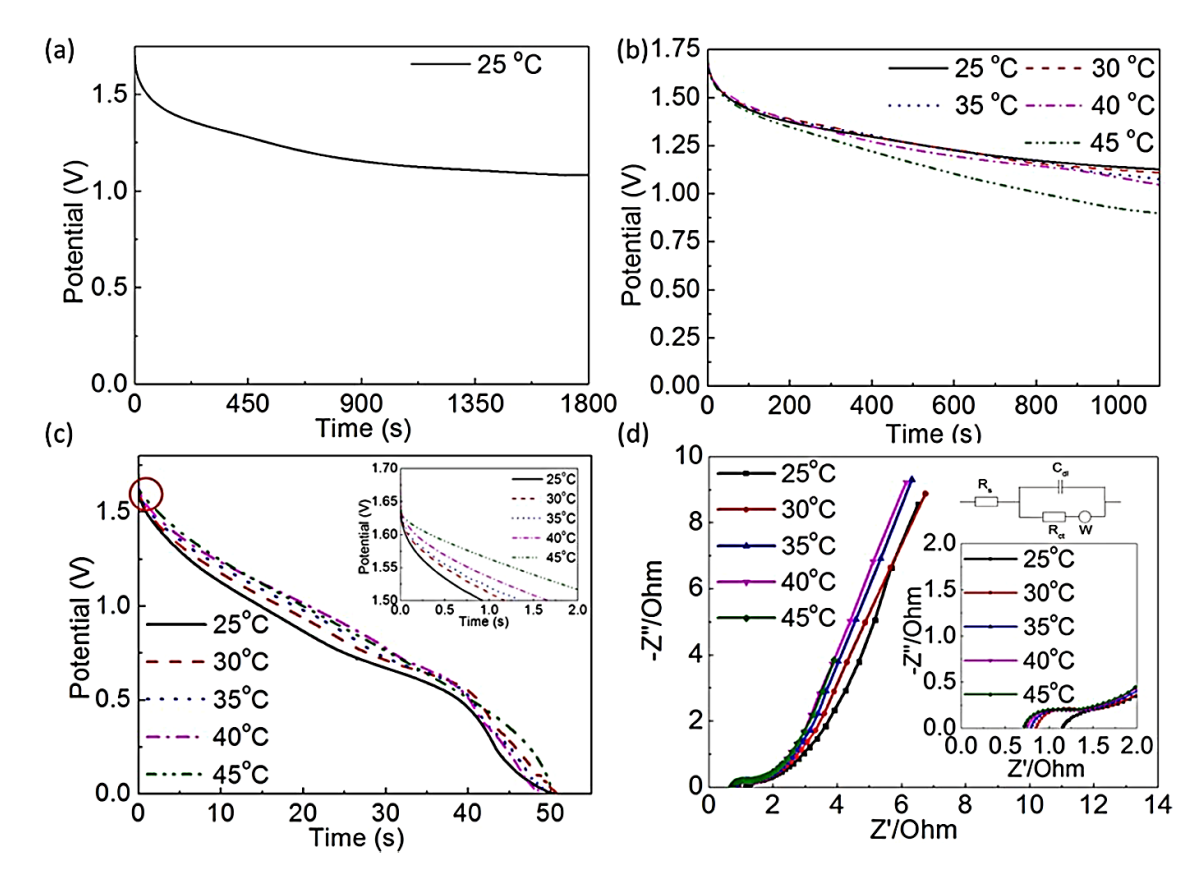


Figure 8. (a). Pacemaker supercapattery self-discharge curves at various temperatures from 25°C to 45°C; (b). a plot of forward anodic peak current density and the square root of the scan rate for CP/NF at various temperatures from 25 to 45 °C; (c, d). discharge curves (at 40 mA/cm²), and Nyquist plots (with equivalent circuit and magnified view of the graph); (a-d). Reproduced with permission copyright 2019, American Chemical Society [114]

Similar to multi-metal oxides, multi-metal phosphides are employed for enhanced redox active sites [108][115][111][112]. Alam et al. [108] synthesized bi-metallic phosphates of NiMn(PO₄)₂ using the sonochemical method. The CV curve (Figure 9) shows that the area under the curve for NiMn(PO₄)₂ was higher as compared to Mn(PO₄)₂ and Ni(PO₄)₂.

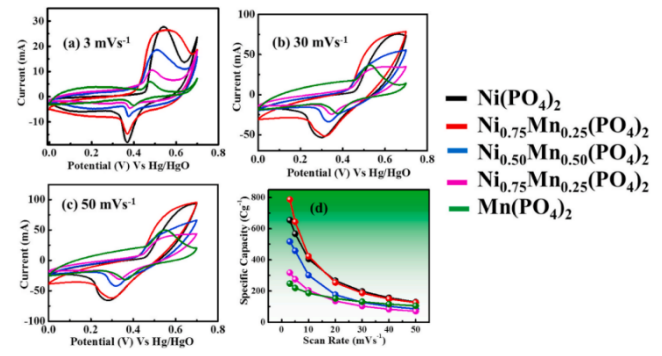


Figure 9. CV curves of all samples with varying Mn content in Ni: (a). at 3 mV/sec; (b) 30 mV/sec; (c). 50 mV/sec; (d). evaluation of specific capacity in relation to scan rates across all samples; (a-d). Reproduced with permission copyright 2021, Elsevier [108]

Additionally, the biphosphate was employed as positive electrode and AC as negative electrode for supercapattery investigation. The device was found to have a good E_s of 63.8 Wh/kg and a P_s of 11,892 W/kg due to the presence of both electrostatic capacitive and

diffusive charge storage mechanism [108]. Alam et al. [111] further enhanced the electrochemical properties of the NiMn(PO₂)₄ by insertion of the PANI matrix as a conducting polymer. NiMn(PO₄)₂-PANI-based ternary composites were synthesized using the facile sonochemical method. The inclusion of PANI in the NiMn(PO₂)₄ composites increases the reversibility of electrochemical reactions in redox processes and provides electroactive sites for ion diffusion. Thus, the supercapattery assembly demonstrates an E_s of 71 Wh/kg and the P_s of 12686 W/kg. Additionally, the device offers a cycle stability of 97.6% after 5000 GCD cycles [111]. Among the most important problems in metal phosphates that need to be resolved are the need of optimal bandgap, structural flexibility, electrical conductivity, and carrier mobility [108].

 Transition metal sulphides have gained a lot of consideration because of their overall high conductivity and high electrochemical performance making these materials capable of storing high energy. Metal sulphides of nickel, manganese, and cobalt show the highest electrochemical properties. Like multi-metal oxides, multi-metal sulphides provide abundant electrochemical active sites that increase the reaction kinetics and electrochemical activity of the device [116]. In order to further increase the capabilities, composites of metal and multi-metal sulphides with MXene, conducting polymers, and carbonaceous composites are extensively employed for supercapattery devices. MXene possesses a 2D-layered structure that provides massive surface area and excellent electronic properties resulting in substantial partial pseudocapacitance and high double-layer capacitance. Table 4 summarizes the performance of metal sulphide-based supercapatteries.

Surendran et al. [117] created a binder-free electrode with a 3D array of flower-like NiS nanostructures on carbon cloth (CC) using an in situ hydrothermal technique (Figure 10). Nickel sulphides have finely tailored morphologies with high specific surface area, whereas CC is an electroconductive substrate employed to enhance the performance of the material [117].



Figure 10. Illustrative diagram for the intermittent progression of the evolution of 3D flower-like β-NiS nanostructure; Reproduced with permission copyright 2017, John Wiley and Sons [117]

The same group also reported a binder-free electrode of nanoflake-like CoS nanostructure on CC by using an in situ hydrothermal technique. The FE-SEM (Figure 11 a,b,c,d) images show that CoS nanoflakes uniformly distribute over the CC substrate with irregular edges. While the irregular edges provided deeper penetration to the electrolyte that improved the active surface area and electrical conductivity, essential for obtaining high electrochemical activity, the uniformity allows enough space for rapid ion transfer.

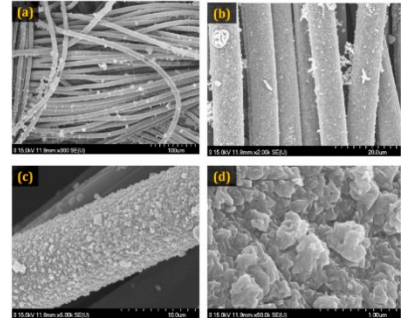


Figure 11. FESEM images of the CoS//CC with varying magnification levels: (a). 100μm; (b). 20 μm; (c). 10 μm; (d). 1 μm; (a-d). Reproduced with permission copyright 2019, Elsevier [118]

The CoS//CC electrode achieved a specific capacitance of 937 F/g having a plateau region in the GCD curve related to its battery-like behaviour. For supercapattery analysis, the CoS//CC and rGO were employed as positive and negative electrodes, respectively. The assembly showed a specific capacitance of 127 C/g and an energy density of 38 Wh/kg. The device also delivered a consistent capacity for ~5000 cycles [118]. Wang et al. [119] synthesized NiCo₂S₄ using the hydrothermal method and the synthesized samples were exposed to a plasma generated by a dielectric barrier discharge in different time intervals. It was observed that the 30 second exposure to plasma generated an abundant amount of sulphur vacancies (Figure 12) and resulted into the reduction of Nickel and Cobalt valence states in NiCo₂S₄ nanostructure leading to higher specific capacitance (782 F/g) as compared to the pristine NiCo₂S₄ (590.4 F/g). Additionally, due to the plasma treatment, tiny voids were created in the material's interior that could better withstand the NiCo₂S₄'s volume change during the faradic charge transfer process, which boosts reaction kinetics. A supercapattery device was fabricated using plasma-induced NiCo₂S₄ (positive electrode) and AC (negative electrode), which delivered a high E_s of 181.75 Wh/kg with a capacitance retention of 91% over 10,000 cycles [119].

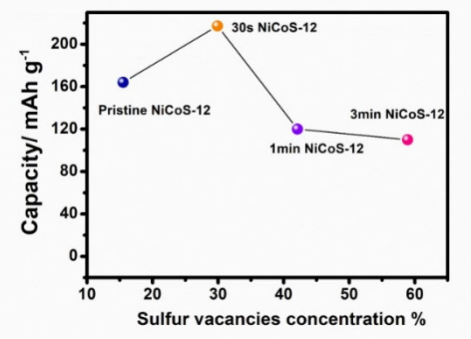


Figure 12. Specific capacity at 0.5 A/g vs S-vacancies concentration plot of NiCoS-12 at different plasma treatment duration; Reproduced with permission, Royal Society of Chemistry [119]

Nasrin et al. [120] synthesized MnCo₂S₄(MCS)@MXene composites using an effective hydrothermal method. MCS nanostructure shows fast electron transfer with considerable redox reactions of electrolytic ions that increase the electrochemical activity of the device. Integration of MCS particles between the MXene layers provides synergetic effect by avoiding the restacking of MXene layers which enlarged the interlayer spacing and boosted the diffusion of electrolyte ions with improved conductivity (Figure 13).

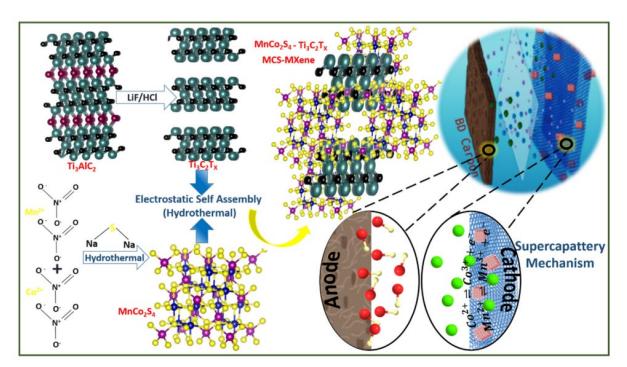


Figure 13. MCS@MXene hybrid material synthesis and supercapattery mechanism are shown schematically; Reproduced with permission copyright 2021, Elsevier [120]

CV curve of the MCS@MXene has a quasi-rectangular shape that shows dominant capacitive behaviour by MXene which is also confirmed by the smaller plateau region in the GCD curve. For supercapattery analysis, MCS@Mxene and aloevera-derived AC were assembled as positive electrode and negative electrode, respectively. The assembly shows a capacitance of 600 C/g at 1 A/g and a very prominent capacitance retention of 100% over 12,000 cycles [120].

Table 2. Metal oxides and their composites as an electrode material for the fabrication of supercapattery

Cell configuration	Specific capacity (C/g)	Energy density (Wh/kg)	Power density (W/kg)	Cycle life	Ref.
α-Ni(OH) ₂ //AC (activated carbon)	246 F/ g (2 A/g)	49	696	87 % over 2000 cycles	[96]
Co ₃ O ₄ //1 KOH//rGO	620 mAh/g	40	742	97.8 % over 5000 cycles	[24]
CeO ₂ //1KOH//rGO	400 (1 A/g)	20	1475	,	[18]
Bi ₂ O ₃ //graphite	559 F/g (0.4 A/g)	8	2040	80% over 5000 cycles	[121]
Fe ₃ O ₄ @N-PCNR//rGO	495 (1 A/g)	46	750	80% over 10,000 cycles	[27]
SrO@PANI//AC	258 (0.8 A/g)	24	323	114% over 3000 cycles	[19]
NiMoO4 NFs@NS//AC	1989 F/g (3 mA/cm ²)	13.2	1644	104% of over 5000 cycles	[20]
2-D MoO _{3-x} //6 M KOH//rGO	573.7 Ah/g (1 A/g)	129.6	11600	98.6% over 10,000 cycles	[97]
$Mn_{0.4}Ni_{0.1}Co ext{-}OA ext{//}AC$	1141.6 (1 A/g)	32.2	770.2	88.1% over 15,000 cycles	[93]
CoMn ₂ O/NG substrate	527 (1 A/g)	44.1	992.6	90.1% of over	[99]

CNT-CuCo ₂ O ₄ @Ag//AC	590 mAh/g (0.5 A/g)	50	4200	10,000 cycles 98% of over 20,000	[21]
Co ₃ O ₄ @C composite//PVA- KOH//AC	138 F/g			cycles	[104]
CoMoO ₄ //AC	64 (1 A/g)	18.89	10600	~93% over 5000	[100]
Co ₃ O ₄ //AC	108.8 (0.3 A/g)	23.7	307	cycles 88.5% over 2500	[122]
rGO-Co ₃ O ₄ -Ag-NPs//AC	115.8 (0.6 A/g)	23.63	440	cycles 85.5% over 3000	[123]
Ni/NiFe ₂ O ₄ @C//rGO	1710 (2 A/g)	62	3440	cycles 100 % over 5000	[22]
$Bi_2MoO_6//Bi_2MoO_6$	485 F/g (5 A/g)	45.6	989	cycles 82% over 5000	[91]
Co(OH) ₂ /Co nanosheets//AC	111 (0.5 A/g)	10	300	cycles. 69.6 % 5000	[98]
CuFe ₂ O ₄ –NR@NiFe ₂ O ₄ – NS//PVA-KOH//rGO	1366 (1 A/g)	72	287	cycles 97% over 10,000	[124]
Li ₂ MnSiO ₄ /Al ₂ O ₃ //AC	141.5 F/g (1 A/g)	12.5	4020.8	cycles 93.6 % over 100	[125]
LiClO ₄ //AC				cycles	[126]
NiO-In ₂ O ₃ (1:2)	766.65	26.24	1752.8	98 % 50,000	[127]
CuCoO ₄ //AC	708 (1 A/g)	19.77	7910.4	cycles 89% over 20000	[128]
Ni/NiO/NC//rGO		37	2750	cycles	[129]
SiC/BiCoZnOM//1 KOH+1 M Na ₂ SO ₄ //SiC/BiCoZnOM	841.1 (1 A/g)	76.25	19000	84.2% over 10000	[130]
MnCo ₂ O ₄ //AC	152.7 mAh/g (5	33.8	318.9	cycles. 85 % over 10,000	[131]
CoNiWO ₄ //AC	mA/cm ²) 626.4 F/g (1 A/g)	42.2	1047.7	cycles 105.3% over 10,000	[132]
Co ₃ O ₄ //AC	171.8 mAh/g (1 A/g)	45.8	725	cycles 83.4 % over 10, 000	[133]
CuCo ₂ O ₄ /Ni ₄ Mo/MoO ₂ @ALD-Co ₃ O ₄ //AC	367.6 (3 A/g)	110.4	2184	cycles 20,000 cycles	[134]
Li ₂ TiO ₃	317 F/g (1 A/g)			95% over 500 cycles	[135]

Ag/Co ₃ O ₄ @PANI//AC	262 (3 mV/sec)	14	165	121.03% over 3500 cycles.	[136]
Graphene-NiO//Activated charcoal	243 (3 mV/sec)	47.3	140	98.7% over 5,000 cycles.	[105]

Table 3 Applications of metal phosphates as electrode materials in the design of supercapattery

Cell configuration	Specific capacity (C/g)	Energy density (Wh/kg)	Power density (W/kg)	Cycle life	Ref.
Strontium phosphide@PANI//AC	196 (0.4 A/g)	28.9	1020	149% over 2000 cycles	[137]
NiMn(PO ₄) ₂ //1 M KOH//AC	678 (0.4 A/g)	63.8	11892	99.2% over 5000 cycles	[108]
Cobalt phosphate//AC	147.2 (0.5 A/g)	34.8	425	87.2% over 10,000 cycles	[109]
rGO//ZnP-rGO	102.78 (0.6 A/g)	24.26	2550	71% over 2000 cycles	[22]
g-C ₃ N ₄ doped vanadyl phosphate	498 (1 A/g)			72% over 5000 cycles	[138]
Cobalt phosphate//AC	1990 F/g (5 mA)	43.2	5800	68% over 100,000 cycles	[114]
$Co_3(PO_4)_2 \cdot 8H_2O//AC$	111.2 F/g (5 mA/cm ²)	29	4687	77.9% over 1000 cycles.	[110]
Ni ₂ P//AC	206 mAh/g (5 mA/cm ²)	42	2856	10000 cycles	[139]
CNF/NiCoP//CNF/NiCoP	269 F/g (1.5 A/g)	36	1200	25 000 cycles	[115]
g NiMn(PO ₄) ₂ -PANI//AC	847 (0.5 A/g)	71.3	12 686	97.6% over 5000	[111]
CuMnPO ₄ //AC	247 F/g (1 A/g)	55	6400	90% over 2500 cycles	[113]
ZnCoMn(PO ₄) ₂ //AC	1704.21 F/g (1.2 A/g)	45.45	4250	93% over 1500 cycles	[112]
Co ₃ (PO ₄) ₂ @PANI	638 (0.8 A/g)	53.2	6027	97.6% over 5000 cycles	[140]

Table 4. Applications of metal sulphates as electrode materials in the design of supercapattery

Cell configuration	Specific capacity (C/g)	Energy density (Wh/kg)	Power density (W/kg)	Cycle life	Ref.
CoS@CC//rGO,	127 (1 A/g)	38	533	5000 cycles	[118]

MnCo ₂ S ₄ @MXene	600	25.6	6400	100% 12,000 cycles.	[120]
β-NiS@CC//rGO	827 (1 mA/cm ²)	38	800	oj erezi	[117]
CuCo ₂ S ₄ @Ni//AC	160.4 F/g (1 A/g)	50.125	750.04	98.6 % after 5000 cycles	[141]
CuCo ₂ S ₄ @Ni//AC	578 (5 mA/cm ²)	51.8	1039	90.8 % 5000 cycles	[142]
NiCo sulfide@selenide//AC	190	39.6	1501	80 % 5000 cycles	[143]
MnO ₂ CoS//AC	781.1 (2 mA/cm ²)	34.72	597.24	89.6% over 9000 cycles	[144]
NiCuS//AC	688 C/g (2 A/g)	23	388	84% over 5000 cycles	[145]
CuS/CoS	138.75 mAh/g (1 A/g)			94.28% over 4000 cycles.	[92]
CuS@Cu ₂ O	145 mAh/g	52 Wh/kg	750 W/kg	80% over 2000 cycles	[146]
$MoO_3Ni_3S_2/NF-0.5/\!/AC$	1.47 C/cm ² (5 mA/cm ²)	4.18 mWh/cm ²	0.34 mW $/\text{cm}^2$	90.5% over 7000 cycles	[147]
NiCoS//AC	215.3 mAh/g (1 A/g)	181.75 Wh/kg	694.3 W/kg	91 % 10,000 cycles	[119]

However, some of the crucial problems that need to be solved involve the optimization of several characteristics, including electrical conductivity, structural flexibility, and band gap. Despite the advancement in supercapattery technologies at a rapid pace, the aforementioned materials are still facing many challenges such as insufficient capacitance, and low-rate capability. Also, they are inept to handle the current energy demands.

Hence, attaining supreme energy and power densities is still a big task for supercapattery devices. MOFs appear as promising candidates to cope up these issues to a great extent due to their unique morphology and outstanding stability.

4. Supercapatteries based on metal-organic frameworks

 MOFs provide a reliable solution for high-rate performance, enriched redox-active sites, multi-electron transportation ways, and fast electrolyte diffusion channels as compared to the aforementioned materials. Due to the distinct features related to high specific surface area and tuneable porosity of MOFs, these materials have drawn attention for use in energy storage and conversion. MOFs are inorganic-organic hybrid porous materials consisting of metal ion linked by organic groups, forming a crystalline, nanoporous structure. MOFs may be able to compete with activated carbon electrodes in EDLCs due to their excellent surface area over 7000 m²/g, which is greater than that of activated carbons. The output of the device is greatly improved by the morphology of MOFs in terms of capacity and rate performance. As a result, MOFs have been explored as potential material for the synthesis of electrode materials for supercapattery.

4.1. Synthesis and characteristics of MOFs

The multitude of MOF synthesis methods aim at developing well-defined inorganic/organic building blocks without causing the organic linkers to break down. Simultaneously, the nucleation and development of the targeted phase are needed that require appropriate kinetics of crystallization [148]. Proper selection of starting materials and reaction conditions is crucial for the synthesis of MOF materials to obtain the desired morphologies. So far, an extensive range of synthesis methods have been furnished such as solvothermal, sonochemical, mechanochemical, and other similar processes. The availability of a large number of synthesis techniques and the choice of starting material makes it a diverse class of material to work with. So far, numerous MOF materials, including MOF-5 [149], MIL-88B [150], MOF-74 [151], ZIF-67 [152], ZIF-78 [153], ZIF-8 [154], and countless others have already been created.

The multifunctional properties of MOFs make them a wise choice for EES applications. Due to their extremely low intrinsic conductivities, pure MOFs are typically regarded as being insufficient. Recently, 2-dimensional (2D) MOFs have been developed that not only have a large specific surface area but also have a high level of electronic conductivity in their purest form [155]. In-plane charge delocalization and extended pi-conjugation, which are facilitated by an electronic network through metal nodes, cause the conductivity in 2D MOFs [156]. To obtain further desired results, MOFs tend to be integrated with other suitable materials. However, inclusion should be done in such a way that it should not lead to a decline in their properties [157]. In this regard, modification in the structure of MOFs can be done in two different ways, i.e., during the synthesis or through post synthesis methods. In the former method, befitting materials are infused at the time of the synthesis of MOFs. Due to the exceptional bonding with the inorganic component or the organic linker, this approach produces a highly stable functional structure [158]-[160]. This strategy not only help in reaching the anticipated levels of conductivity but also has synergistic benefits on performance as a whole by enhancing the properties of individual components [161], [162]. Similarly, in later case, the post-synthesis modification is also implemented to meet the desired requirements. Integration of MOFs and other innovative materials like graphene oxide, reduced graphene oxide, MXene, metal oxides, transition metal dichalcogenides (TMDs), quantum dots, carbon nanotube, conducting polymers, and mixed metallic MOFs were evaluated critically [163]–[166]. Due to their ability to maintain an appropriate pore size distribution, which is necessary for the creation of competent supercapattery electrodes, these composites have become a popular choice [167], [168]. The subsections given below present the important developments made in transforming MOFs into more electrochemically active materials that are desirable for supercapattery applications.

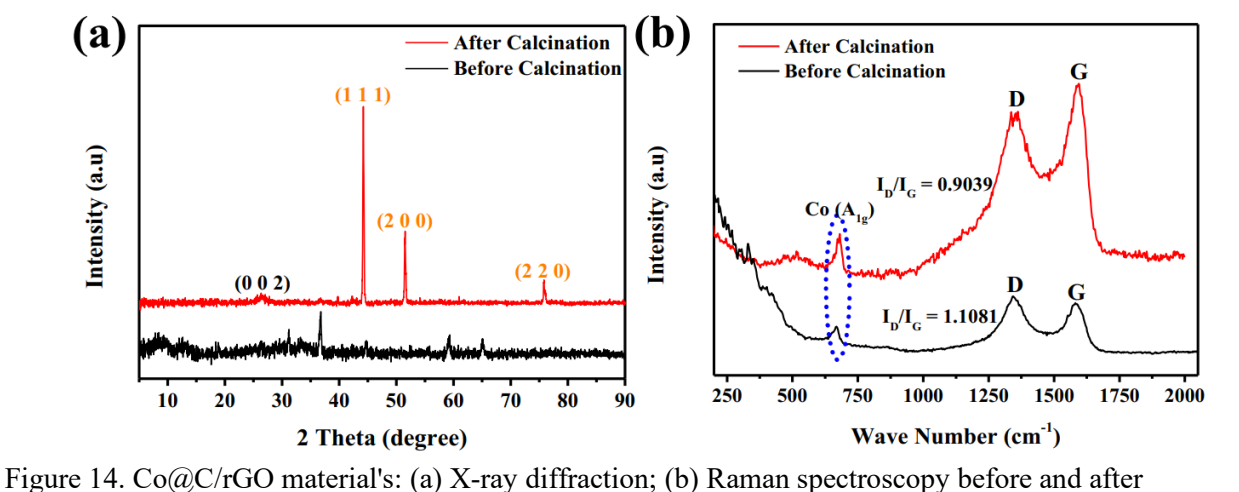
4.2. MOF derivatives based supercapattery

MOFs are used as precursors or sacrificial framework to derive the nanomaterials that inherit the structural cage-like properties of parent MOFs with high specific surface area and a rich porous structure. MOF-derived sulphides, oxides, phosphides, and nanoporous carbon are helpful for the enhancement of specific capacitance and rate capability of the electrode materials. In comparison to traditionally available activated carbon and metal oxides, pyrolysis of MOFs in an inert environment to create nanoporous carbon (NPC) structures [169]–[173] or in air to create metal oxides preserves the high specific surface area qualities while also providing the conductive frameworks [12]. Conversion into sulphides or phosphides in the presence of different reducing agent (thioacetamide, sodium sulphide, NaPO₂H₂·H₂O, etc.) not

only enhances the conductivity but also provides the porous framework for an enhanced stability.

The most popular choice of metals for supercapattery electrodes are Nickel and Cobalt. Ni-MOFs as electrode material possess high specific capacitance (C_s) but the rate capability is low, whereas Co-MOFs possess a low value of C_s with outstanding rate capabilities. As an effective method to overcome these limitations, Ni and Co metal ions are integrated together into MOF texture, which enhances the overall electrochemical performance [174]. To further improve the electrochemical properties, Ni, Co, and bi MOFs have been used as a precursor for obtaining various derivatives ranging from hydroxides, sulphides, and oxides [175]–[177]. The highly porous and hollow frameworks of metal oxides, hydroxides, sulphides, or phosphides derived from MOFs offer shorter paths for the electrolyte ions diffusion, facilitating near-surface and surface redox reactions with a striking enhancement in the reaction kinetics. Other than this, activated carbon is the most suitable counter electrode for supercapattery due to its high abundance, low cost, and good conductivity having a potential window of (-1 to 0 V) [178], [179] which enhances the overall potential window of supercapattery device. The most widely used electrolyte for MOF-derived supercapatteries is KOH because of its abundant ionic concentrations, low resistance, and smaller ionic radius [175]–[179]. Table 5 summarizes the performance of metal oxide-based supercapatteries.

Wu et al. [177] synthesized carbon nanoparticles (NPs) of approximately 100 nm size derived from Co MOF using one-pot hydrothermal process. The uniform and suitable size of Co particles contributed to maximising the intrinsic faradaic reaction characteristics of Cobalt. Additionally, graphitized carbon peak is absent from the XRD curve of Co MOF-derived NPs (Figure 14 a), indicating poor crystallisation, which is further supported by Raman spectra (Figure 14 b), and results in better electrical conductivity [180].



calcination; (a,b). Reproduced with permission copyright 2022, Elsevier [180] Further, these nanoparticles were anchored on 3D rGO aerogel sheets to construct electric network for Co MOF-derived carbon matrix that facilitates ion diffusion during charge and

discharge processes. Figure 15 of the SEM and TEM images demonstrates that the rGO has large-sized, highly transparent layers that aide in increasing specific surface area, electrical conductivity, and double-layer capacitance, all of which help to support long-term cyclic

stability [179].

1

2

3

4

5

6 7

8

9

10

11

12 13

14

15

16 17

18

19 20

21

22 23

24 25

26 27

28

29

30

31

32

33

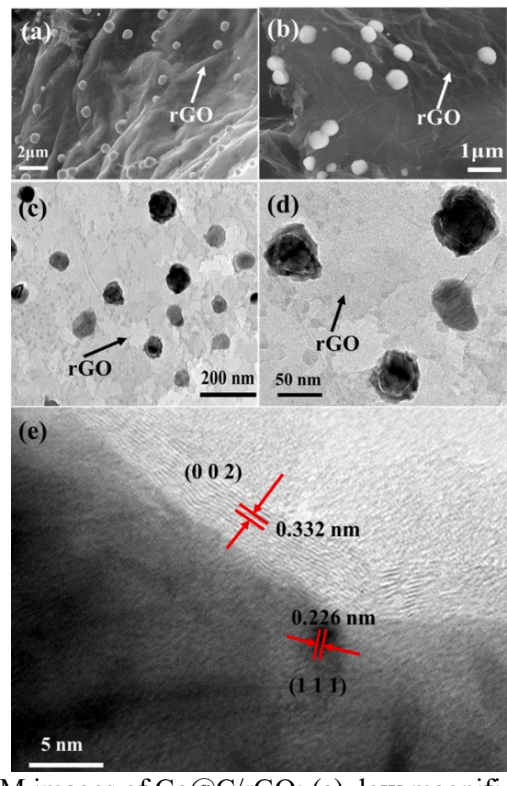


Figure 15. SEM and TEM images of Co@C/rGO: (a). low magnification SEM picture taken before calcination; (b). high magnification SEM image; (c). low magnification TEM image taken before calcination; (d). High magnification TEM image; (e). high resolution TEM image taken after calcination; (a-e). Reproduced with permission copyright 2022, Elsevier [177]

For supercapattery applications, Co@C/rGO (positive electrode) and AC (negative electrode) combination provides a specific capacitance of 810 C/g (current density of 1 A/g), delivered a high E_s of 29.5 Wh/kg at a P_s of 720 W/kg, and a very high capacitance retention of 93.7% after 10,000 cycles [177]. Karuppasamy et al. [179] synthesized polyhedrons structure of NiCo alloy derived from MOF on graphitic carbon nanostructure. In comparison to mono Ni@GC and Co@GC, the polyhedron structure of NiCo offers adequate routes for ionic migration and speeds up the fast charging-discharging of active species that is useful in delivering high specific capacity and coulombic efficiency with enhanced electrochemical performance (Figure 16). NiCo@GC material's surface-active sites participate in the electrochemical reactions, but its intrinsic active sites are less effective in participating in these reactions at higher current rates, leading to reduced capacitance. For improving the energy storage, a supercapattery was prepared by employing NiCo@GC and AC. This supercapattery exhibited a specific capacity of 74.3 mAh/g with E_S of 39.5 Wh/kg and having coulombic efficiency of 99.95% after 5000 charge-discharge cycles [179].

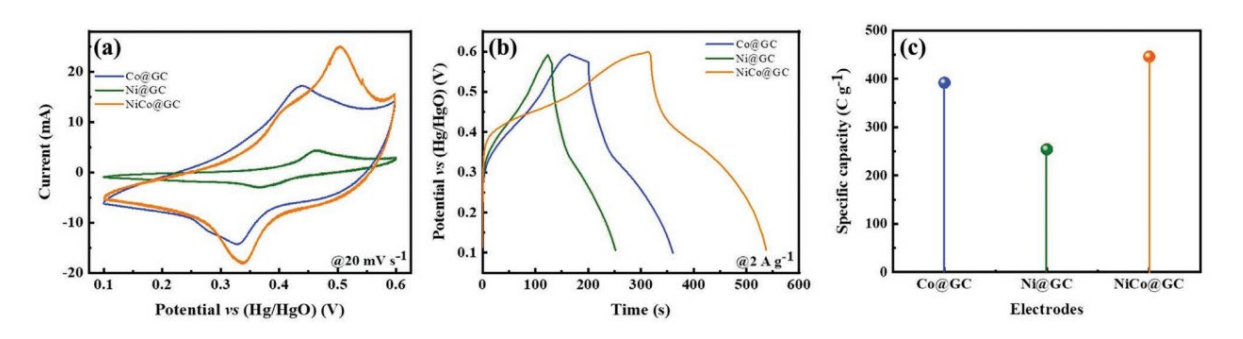


Figure 16. Electrochemical properties of pure Ni@GC, Co@GC, and NiCo@GC-nanostructured electrodes derived from MOFs: (a,b). CV curve at 20 mV/sec, relevant GCD plot at 2 A/g, and (c). comparable capacity curve at 2 A/g; (a-c). Reproduced with permission copyright 2022, John Wiley and Sons [179]

By combining a MOF template driven method with surface amorphization strategy, Jiao-Jiao et al. [176] synthesized NiCo LDH/NiCoB_i (Borate) nanosheet derived from MOF.

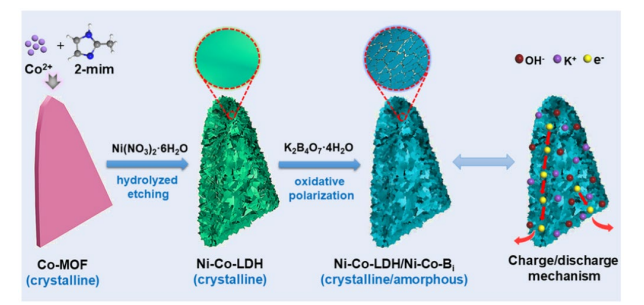


Figure 17. NiCo LDH/NiCo B_i nanosheet array formation process illustrated schematically; Reproduced with permission copyright 2020, American Chemical Society [176]

When used in an electrochemical procedure, the MOF-derived LDHs have the ability to successfully overcome a variety of challenges such as low conductivity and easy aggregation. The NiCo LDH also possess a large number of oxygen vacancies with unsaturated surface atoms that absorb OH and produce a large number of active sites [181]. Therefore, adding NiCo LDH will help create hierarchical composites with improved energy storage capabilities. Additionally, the presence of light weight boron element in the structure coordinates with the oxygen atom of an LDH forming various clusters and further transform borates into different structures. This provides plenty of redox active sites, that fill up the lack of LDHs. The NiCo LDH/NiCo B_i display a specific capacitance of 891 C/g (1 A/g). When assembled as supercapattery, the device shows a 1.8 V potential window and can run an LED for 60 seconds [176].

 Chen et al. [175] synthesized a microarray of composite $\text{Co}_9\text{S}_8@\text{Ni}_3\text{S}_2/\text{ZnS}$ using a simple three-step wet mixing process from MOF. In $\text{Co}_9\text{S}_8@\text{Ni}_3\text{S}_2$ both Cobalt and Nickel cations contributed to the redox reaction that is helpful in improving both rate capability and specific capacity. Whereas the integration of inert Zinc ion promotes cycling stability with enhanced electrocapacitive activity, the incorporation of Ni and Zn ion in Cobalt synergistically enhances the overall performance of the composites.

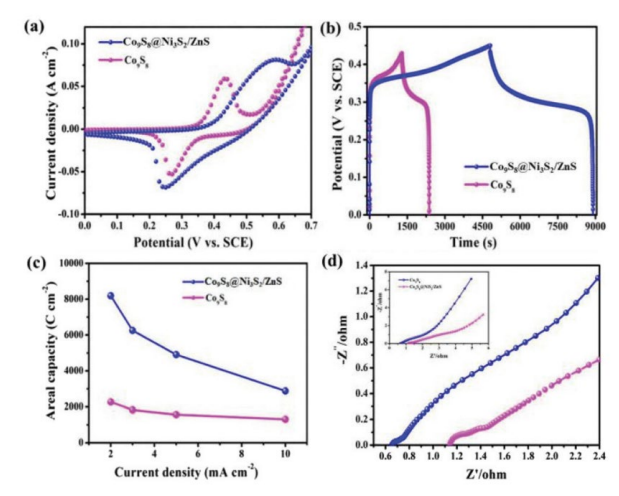


Figure 18. Electrochemical performance of Co₉S₈ and the Co₉S₈@Ni₃S₂/ZnS electrode is compared: (a). CV curves at a scan rate of 5 mV/sec; (b). GCD curves at the current densities of 2 mA/cm²; (c). specific capacity at different current density; (d). Nyquist plot; (a-d). Reproduced with permission, Royal Society of Chemistry [175]

The sample when initially tested in three electrode configuration (Figure 18) showed a capacitance of 8192 C/cm^2 (at 2 mA/cm^2). The resultant $\text{Co}_9\text{S}_8@\text{Ni}_3\text{S}_2/\text{ZnS}$ has a high specific surface area and a mesoporous structure that is helpful in enhancing the electrochemical storage performance of the device by giving abundant reactive sites and improving charge transfer kinetics. For supercapattery applications, $\text{Co}_9\text{S}_8@\text{Ni}_3\text{S}_2/\text{ZnS}$ and AC were employed as positive and negative electrodes, respectively, in gel KOH electrolyte (Figure 19). The assembled device $\text{Co}_9\text{S}_8@\text{Ni}_3\text{S}_2/\text{ZnS}//2 \text{ M KOH}//\text{AC}$ shows a P_s of 1.517 mW/cm² and an E_s of 0.377 mWh/cm² [175].

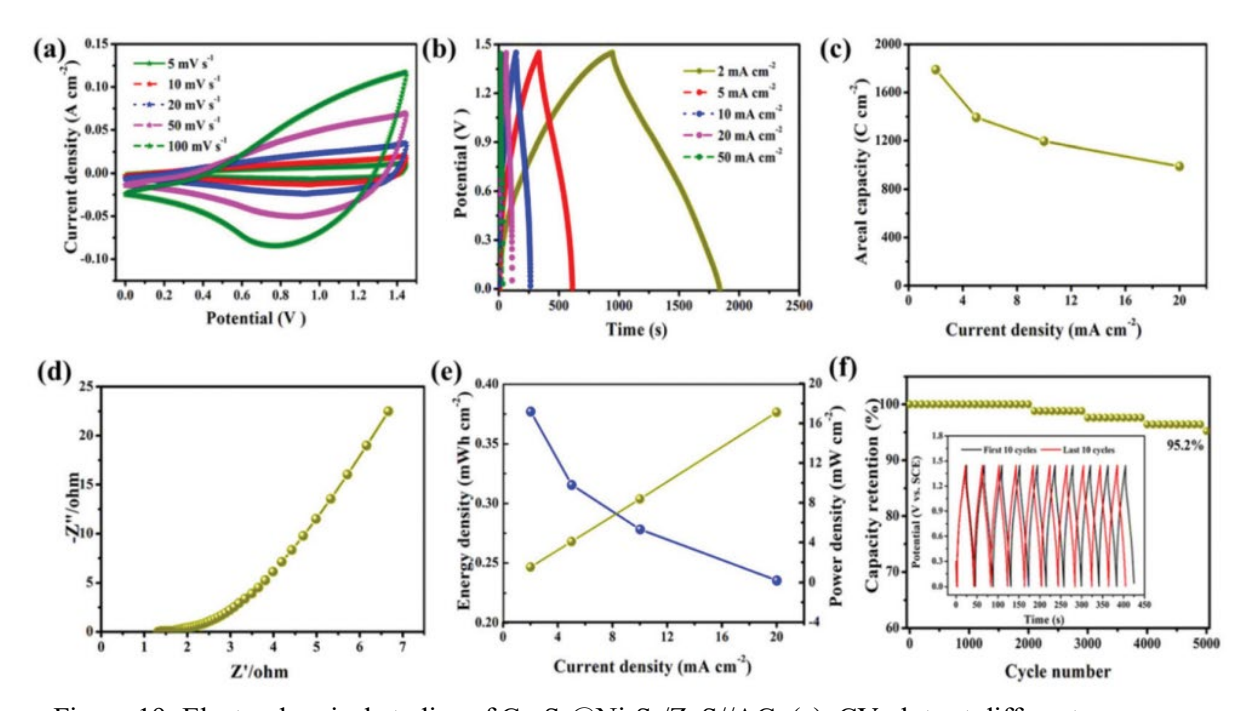


Figure 19. Electrochemical studies of Co₉S₈@Ni₃S₂/ZnS//AC: (a). CV plots at different scan rates; (b). GCD plots at various current densities; (c). the areal capacity at different current density; (d). Nyquist plot (e). the energy density and power density at various current densities; (f). cycling performance; (a-f). Reproduced with permission, Royal Society of Chemistry [175]

1 Table 5. Applications of MOF derived structure as electrode materials in the design of supercapattery

Cell configuration	Specific capacity (C/g)	Energy density (Wh/kg)	Power density (W/kg)	Cycle life	Ref.
Co ₉ S ₈ @Ni ₃ S ₂ /ZnS//2 M KOH//AC	8192 C/cm ² (2 mA/cm ²)	0.377 mWh/cm ²	1.517 mW/cm ²	95.2% over 5000 cycles	[175]
NiCo layered double hydroxide//NiCo borate//2 M KOH//AC	891 (1 A/g)	62.8	800	81% over 5000 cycles	[176]
Co@C/rGO//AC	810 C/g	29.5	720	93.7 % over 10,000 cycles	[177]
fcc-NiCo@Graphitic carbon polyhedron//3 M KOH//AC	444 C/g (2 A/g)	39.5	665	99.95% over 5000 cycles	[179]
NiCoMn (NCM)-based MOF//1M KOH//AC	1311.4 μAh/cm ² (5 mA/cm ²	1.21 mWh/cm ²	32.49 W/ cm ²	100% over 5000 cycles	[178]

High temperatures are typically needed to pyrolyze MOFs into porous carbon, metal oxides, metal sulphides, and metal phosphides. But the treatment at high temperature and pressure might destroy MOFs frameworks, which results in the decrease of the electroactive sites and specific surface area. Integrating MOFs with various materials, such as metal nanoparticles, conducting polymers (PANI, polypyrrole, etc.), quantum dots, metal oxides, and carbon-based materials (e.g., carbon nanotubes, biowaste derived activated carbon), is another way to address this problem.

9 10 11

2

3

4

5

6

7

8

4.3. **MOF** composites based supercapatteries

12 13

14

15

16

17

18

19

20

21

22

23

24

25

26

27

28

29

30

31

Integration of MOFs with composites is very helpful in increasing the low conductivity and poor stability of MOF material with enhancement in efficiency. The properties of composites are mainly governed by synergistic effect of the diverse compositions and structures.

Similar to MOF-derived oxides/hydroxides and sulphides, composites with Ni and Co MOF are extensively employed. They are integrated with carbon materials as they are easy to synthesize, enhance the cross-sections, provide high chemical stability, high-temperature resistance, and good conductivity to the MOFs. Because of this, porous carbon, carbon nanotubes (CNTs), and other activated carbon compounds have been reported for various energy storage devices over the past few years [1], [182]–[185]. Graphene has drawn the most attention of all materials due to its good electrical conductivity, strong thermal stability, and high theoretical capacity with MOFs, another class of materials that are extensively employed with MOFs are conducting polymers. In addition to conductivity, polypyrrole and PANI are often utilised as additive polymers because of their facile synthesis, simple construction, superior mechanical qualities, high tuneable electrical properties, and high environmental resilience [26]. In addition, integration of MOFs with conducting polymers and graphene was found to be suitable for enhancement in the potential window ranging from (1-1.8 V) of supercapattery device. Not only pristine MOFs, but their composites with derivatives are also largely employed to combine the properties of derivatives and additives. Table 6 summarizes the performance of MOF composite-based supercapatteries.

Using a hydrothermal approach, Iqbal et al. [186] created Cobalt MOF@polyaniline (PANI) composites. Polyaniline was synthesized using polymerization of aniline. Addition of PANI in Co MOF enhances electrical conductivity, electrochemical activity, flexibility, and redox properties. After investigations from the BET data of Co MOF@ polyaniline (PANI) composites, the specific area was found to be 156.59 cm²/g, whereas pore size and pore volume were found to be 25.06 nm and 0.9811 cm³, respectively (Figure 20). It demonstrates mesoporosity in the composites, making the composite viable for energy storage applications. The MOF@polyaniline matrix was combined with an AC electrode for the supercapattery. The device gave an output of 104 C/g, an E_s of 23.11 Wh/kg, and a P_s of 6400 W/kg [186].

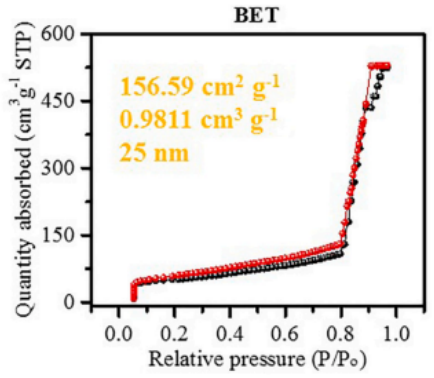


Figure 20. Co MOF@PANI-50/50% BET analysis; Reproduced with permission copyright 2020, Elsevier [186]

Liu et al. [187] used an efficient ultrasonic procedure to create NiCo MOF nanosheets encased in polypyrrole nanotubes (PNTs) at ambient temperature. The incorporation of PNTs with NiCo MOFs improves the capacitive characteristics, boosts electronic conductivity by providing a conductive network, minimizes agglomeration, increases specific surface area, number of active sites, and adds additional pseudocapacitance. The electrodes are initially evaluated in three electrode configuration to assess their electrochemical performance. As observed from the CV and GCD plots, NiCo MOF@PNTs (Figure 21) delivered a specific capacitance of 1109 F/g at 0.5 A/g that is significantly greater than NiCo MOF and PNTs alone. The pore size distributions of NiCo MOF@PNTs are found to be centred at 2-5 nm from BET, which is higher than that of NiCo MOF but smaller than polypyrrole nanotubes. Hence, PNTs are beneficial in enhancing NiCo MOF nanosheets' specific surface area and electrical conductivity, which improves the overall performance. For practical applications, NiCo MOF@PNTs and AC electrode based supercapattery device provided an E_s of 41.2 Wh/kg at a P_s of 375 W/kg. Also, it shows a capacitance retention of 79% over 10,000 charge-discharge cycles. By connecting two supercapattery devices in series, a yellow coloured LED could be lit for 30 mins [187].

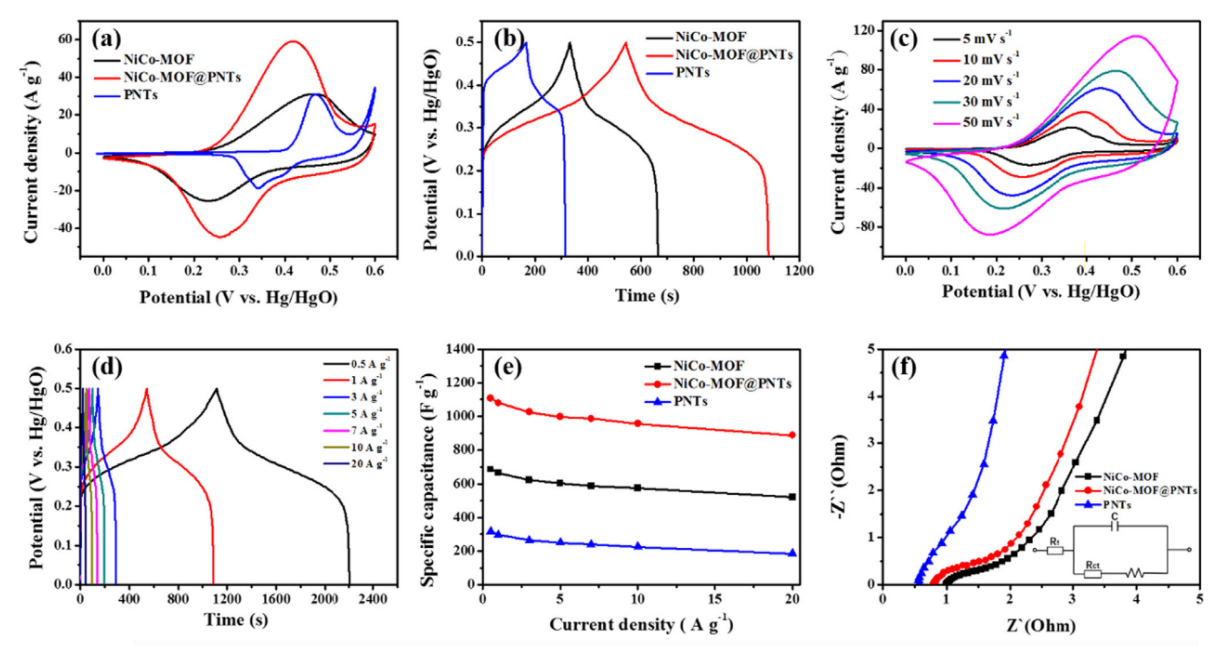


Figure 21. Electrochemical studies of NiCo MOF, NiCo MOF@PNTs, and PNTs are shown: (a). CV curves at a scan rate of 20 mV/sec; (b). GCD curves at 1 A/g; (c). CV curves of NiCo MOF@PNTs at various scan rates; (d). GCD curves of NiCo MOF@PNTs at various current densities; (e). the specific capacitances at various current densities; (f). Nyquist plot; (a-f). Reproduced with permission copyright 2021, Elsevier [187]

Faisal et al. [188] synthesized ZIF-8@terpolymer composite using three steps hydrothermal method. The ZIF particles are distributed well over the surface of the terpolymer crystal, as shown by the TEM and SEM images (Figure 22). Due to the fact that they are building a network of polymeric chains, these crystals were closely attached to one another and were not separated. As a result, the ZIF-8 builds up in the terpolymer framework, increasing its surface area and giving it a mechanical advantage. The supercapattery device delivered an E_s of 38 Wh/kg with a P_s of 1600 W/kg and show 100% capacitance over 1000 GCD cycles [188].

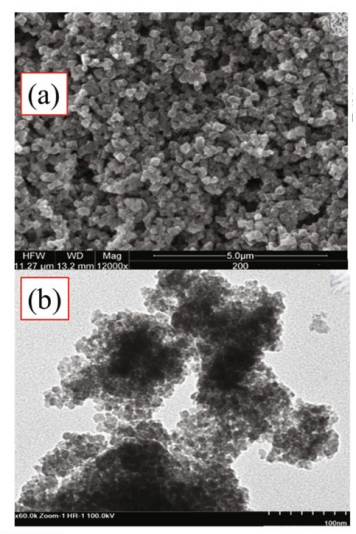


Figure 22. (a). SEM; (b). TEM of ZIF-8@terpolymer; (a,b). Reproduced with permission copyright 2021, Elsevier [188]

Renan et al. [26] synthesized trypan blue-Ni-MOF (Try-Ni-MOF) and Azure (Az) 3D graphene aerogel (GA) (Figure 23) using hydrothermal method. The transport of ions

throughout the material is made possible by the Az-GA with Try-Ni-MOF structure, which improves ion transfer channels and provides increased surface accessibility through electrically active species. For supercapattery application Az–GA and Try–Ni-MOF is employed as positive and negative electrode, respectively. The assembly showed the specific capacitance of 319 F/g at 1 A/g with an E_s of 66.55 Wh/kg and a P_s of 349 W/kg. Moreover, it shows a capacitance retention of 92% after 5000 charge-discharge cycles [26].

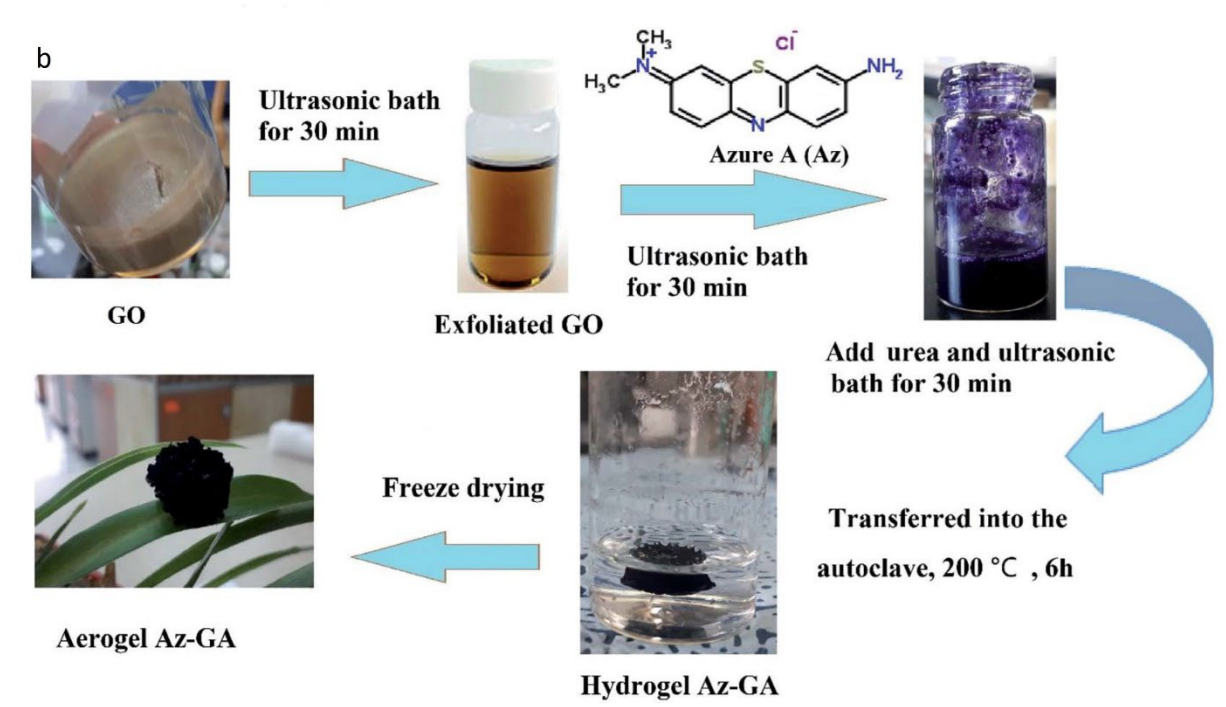
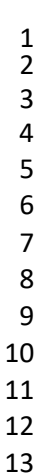


Figure 23. (a). Fabrication of the Try-Ni-MOF; (b). Az-via and a 3D GA are synthesized via a hydrothermal process; (a,b). Reproduced with permission, Royal Society of Chemistry [26]

 Similar hierarchical NiCo-LDH nanostructures were created by Ghosh et al. [28] and supported by rGO nanosheets. During an electrochemical reaction, the layered structure of LDH allows a gradual ion diffusion through the pore channel [181]. The integration of rGO increases the conductance along with enhancing the surface area of the electrodes, which subsequently increases the charge transport mechanism by providing ample active sites. For supercapattery application, NiCo-LDH@rGO was employed as a negative as well as a positive electrode. The assembly provided an E_s of 45.2 Wh/kg and a P_s of 750 W/kg and upholds more than 60% capacity retention even after 3500 cycles. NiCo-LDH@rGO composites exhibit narrow pore size distribution, with an average pore size of 3.8 nm as per the BET measurements and TEM images. Mesoporous structure is thus present in the composites. These porous materials have a large capacity for storing electrolyte on their interior surfaces and shortening the ion diffusion path, which increases the capacitance of electrode materials. By blazing a blue coloured LED for more than 7 minutes, the supercapattery cell further illustrates the practical application of this material [28].

TiO₂ aerogel@Co-MOF composite was synthesized by Ramasubbu et al. [189] for the electrode of supercapattery. TiO₂ aerogels have a 3-dimensional interlinked hierarchical mesoporous continuous architecture that decreases the diffusion path, allows electrolyte ions to diffuse into the pores, and creates upright paths for charge transport. However, the addition of MOF improves power conversion efficiency, extends electron longevity, and lowers charge recombination. As a result, mixing MOFs with TiO₂ aerogel maximises the advantages of both materials. This hierarchical nanostructure provides enriched electroactive sites, a high specific surface area, and a short diffusion channel. According to the XRD results (Figure 24), the TiO₂ aerogel's crystallinity reduces when MOF is added because it inhibits TiO₂ growth and leads to the creation of mixed phases with more structural flaws, which improves electrochemical performance.



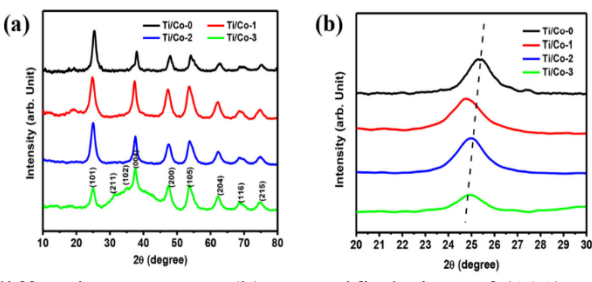


Figure 24. (a). X-ray diffraction patterns; (b). magnified view of (101) of pristine TiO₂ aerogel (Ti/Co-0), and (Ti/Co-1, Ti/Co-2, Ti/Co-3) composites, respectively; (a,b). Reproduced with permission copyright 2020, Elsevier [189]

The materials were initially tested in a 2 M KOH solution in three electrode configurations. In comparison to TiO₂ aerogel (66.4 C/g), TiO₂ aerogel@Co-MOF composites have a higher specific capacitance of 111.2 C/g at 0.8 A/g. It was observed that the integration of MOF improved the mobility of electrolytic ions, resulting in varied electrolyte ionic routes of the electrode materials. For supercapattery applications, TiO₂ aerogel@Co-MOF composite and AC were employed for which the operational potential window was extended to 1.5 V. After 5000 GCD cycles, the device's capacitance retention was found to be 93% [189].

Table 6. Applications of MOF@composites in the design of supercapattery application

Cell configuration	Specific capacity (C/g)	Energy density (Wh/kg)	Power density (W/kg)	Cycle life	Ref.
TiO ₂ aerogel@Co-MOF composite/electrolyte//AC	111.2 (0.5 A/g)	7.5	1875	93% over 5,000 cycles.	[189]
NiCo MOF@ Polypyrrole//KOH//AC	1109 F/g (1 A/g)	41.2	375	79.1% over 10,000 cycles	[187]
Az–GA//1M KOH//Try–Ni-MOF	319 F/g (1 A/g)	66.55	445	92.12 % after 5000 cycles	[26]
Co-MOF@ PANI/1 M KOH/AC	104 (1 A/g)	23.11	6400	100% over 1000 cycles	[186]
Zn-MOF@ terpolymer//1 M KOH//AC	171.15 (0.3 A/g)	38.05	1600	100% over 1000 cycles	[188]
NiCo-LDH using ZIF-67@rGO-30	1658 F/g (1 A/g)	45.2	750.2	60% over 3500 cycles	[28]

5. Conclusion and future perspective

The main aim of this review paper is to provide the latest perspective on supercapattery devices that integrates the advantageous properties of both supercapacitors and batteries in a single supercapattery device. Supercapattery devices offer enhanced electrochemical performance empowering the modern-day necessities of high power, energy densities, and long cyclic stability with a wide potential window. Progress in electrodes with innovative technological advancements and enhanced functional capacities is a vital way to develop new

supercapattery devices with higher energy and power density and this will pave the way to great societal impact. Further, the review covers the current developments in transition metalsbased electrode materials for supercapattery applications, but the specific capacitance, energy/power densities, and cyclic stability of these materials fall short of the acceptable level. Structures generated from metal-organic frameworks (MOFs) and their composites are potential materials for building functional electrodes for supercapattery devices. One of the most compelling factors for researchers to discover varied compositions of MOFs, MOFderived structures, and MOF-composites is the ability of their parameters to be tailored with ease to meet the desired characteristics. This review study establishes that MOFs are extremely beneficial in developing supercapattery electrodes that outperform the currently used batteries and supercapacitors. Higher specific surface area and enriched active sites are offered by MOFderived structures and their composites. Different MOF composites, including conductive polymers, graphene, and MXene help to overcome the low conductivity and unstable nature of MOFs. High power and energy densities combined with superior specific capacitance are provided by MOFs incorporating cobalt, nickel, and other metals. In conclusion, the potential of MOFs for supercapattery applications has not yet been fully explored. Fundamentally, this field needs additional investigations. MOF-derived sulphides/phosphides and composites of MOF with state-of-the-art efficient materials like MXene, metal dichalcogenides, and perovskites can be utilized for the supercapattery applications.

Currently some MOFs are already available in the market but impose huge costs. It may be difficult, but not impossible, to create facile and economical processes that produce MOF materials at low cost to fully realise their potential for supercapattery applications. Additionally, it is crucial for MOFs to undergo rigorous charge-discharge tests (at least >100000 cycles) to ensure that they meet the practical standards for commercial carbon electrodes. Therefore, major research should be done in future to modify the synthesis methods of MOF-based structures and improve their processability for commercial applications. Finally, to maximise the electrochemical performance of MOF-based nanostructures for supercapattery, a better comprehension of the charge-discharge mechanisms needs to be explored through material informatics. Further, use of artificial intelligence and simulation studies may pave the way for a faster optimization of parameters through predictive analysis which may led to better utilization of resources. This review must inspire researchers to develop metal-organic framework inspired structures and explore their potential for high performance supercapattery electrodes.

Acknowledgement

 Author Megha Prajapati is grateful to Indira Gandhi Delhi Technological University for Women (IGDTUW) for providing financial support for her research work.

List of Abbreviations

41	SCs	Supercapacitors
42	EES	Electrochemical Energy Storage
43	EDLC	Electric Double Layer Capacitors
44	MOF	Metal Organic Framework
45	AC	Activated Carbon
46	CNT	Carbon Nanotubes
47	C^{sp}	Specific Capacitance
48	Q	Charge Store
49	ΔU	Potential Range

1 m Effective Mass 2 E_s Energy Density 3 P_s Power Density 4 NP Nanoparticles

5 rGO Reduced Graphene Oxide

6 TMD Transition Metal Dichalcogenides

7 NPC Nanoporous Carbon

8 ECPs Electrically Conducting Polymers

9 TMOs Transition Metal Oxides

PEDOT Poly (3,4-ethylene dioxythiophene)

11 PNT Polypyrrole Nanotubes12 CV Cyclic Voltammetry

13 GCD Galvanostatic Charge Discharge

14 EIS Electrochemical Impedance Spectroscopy

15SEMScanning Electron Microscopy16XRDX-ray Diffraction Spectroscopy17XPSX-Ray Photoelectron Spectroscopy18EDXEnergy-Dispersive X-Ray Spectroscopy19TEMTransmission Electron Spectroscopy

20 BET Brunauer–Emmett–Teller

21 Az Azure

22 GA Graphene Aerogel
23 PANI Polyaniline
24 Ppy Polypyrrole
25 GC Graphitic Carbon

26 LDH Layered Double Hydroxide

27 CCCarbon Cloth 28 1-D One Dimension, 29 Two Dimensions 2-D 30 3-D Three Dimensions 31 RuO₂ Ruthenium Dioxide 32 MnO_2 Manganese Dioxide 33 Co₃O₄ Cobalt Tetraoxide 34 V_2O_5 Vanadium Pentoxide

35 Fe₃O₄ Ferric Oxide 36 SnO₂ Tin Oxide

37 NaBH₄ Sodium Borohydride

38 LiAlH₄ Lithium Aluminum Hydride

MoO Molybdenum Oxide
 Ni(OH)₂ Nickel(II) Hydroxide
 KOH Potassium Hydroxide
 Co₃O₄ Cobalt Tetraoxide
 CeO₂ Cerium Oxide

44 Bi₂O₃ Bismuth Trioxide 45 Fe₃O₄ Ferric Oxide

46 N-PCNR N-Porous Carbon Nano Rice

47 SrO Strontium oxide
48 NF Nanoflowers
49 NSs Nanosheets
50 NiMoO₄ Nickel Molybdate

51 Mn_{0.4}Ni_{0.1}Co-OA Manganese Nickel Cobalt Oxalate

NG
 Nitrogen-doped Graphene
 CuCo₂O₄
 Copper Cobaltite
 PVA
 Polyvinyl Alcohol

55 CoMoO₄ Cobalt Molybdate

Ag Silver
 NiFe₂O₄ Nickel Ferrite
 Bi₂MoO₆ Bismuth Molybdate
 Co(OH)₂ Cobalt hydroxide

60 NiFe₂O₄ Nickel Ferrite

1	NR	Nanorods
2	$CuFe_2O_4$	Copper Ferrite
3	Li ₂ MnSiO ₄	Lithium Manganese Silicates
4	Al_2O_3	Aluminium Oxide
5	LiClO4	Lithium Perchlorate
6	NiO	Nickel Oxide
7	In ₂ O ₃	Indium oxide
8	Li ₂ TiO ₃	Lithium Titanium Oxide
9	$NiMn(PO_4)_2$	Nickel Manganese(II) phosphate
10	$g-C_3N_4$	Graphitic Carbon Nitride
11	Ni_2P	Di Nickel Phosphide
12	CNF	Carbon Nano Fibre
13	ZnCoMn(PO ₄) ₂	Zinc Cobalt Manganese phosphate
14	CoS	Cobalt sulfide
15	NiS	Nickel Sulfide
16	$CuCo_2S_4$	Copper Cobalt Sulfide
17	NCM	NiCoMn
18	ZIFs	Zeolitic imidazolate frameworks
19	TiO_2	Titanium dioxide
20	GA	Graphene Aerogel
21	MIL N	Matériaux de l'Institut Lavoisier
22		
23		

26 References

24

- 27 [1] M. S. Rahmanifar, H. Hesari, A. Noori, M. Y. Masoomi, A. Morsali, and M. F.
 28 Mousavi, "A dual Ni/Co-MOF-reduced graphene oxide nanocomposite as a high
 29 performance supercapacitor electrode material," *Electrochim. Acta*, vol. 275, pp. 76–
 30 86, 2018, doi: 10.1016/j.electacta.2018.04.130.
- T. Kim, W. Song, D. Y. Son, L. K. Ono, and Y. Qi, "Lithium-ion batteries: outlook on present, future, and hybridized technologies," *J. Mater. Chem. A*, vol. 7, no. 7, pp. 2942–2964, 2019, doi: 10.1039/C8TA10513H.
- H. Zhang, C. Mao, J. Li, and R. Chen, "Advances in electrode materials for Li-based rechargeable batteries," *RSC Adv.*, vol. 7, no. 54, pp. 33789–33811, 2017, doi: 10.1039/c7ra04370h.
- S. Saffirio, M. Falco, G. B. Appetecchi, F. Smeacetto, and C. Gerbaldi,

 "Li1.4Al0.4Ge0.4Ti1.4(PO4)3 promising NASICON-structured glass-ceramic

 electrolyte for all-solid-state Li-based batteries: Unravelling the effect of diboron

 trioxide," *J. Eur. Ceram. Soc.*, vol. 42, no. 3, pp. 1023–1032, 2022, doi:

 10.1016/j.jeurceramsoc.2021.11.014.
- F. Boorboor Ajdari *et al.*, "A review on the field patents and recent developments over the application of metal organic frameworks (MOFs) in supercapacitors," *Coord. Chem. Rev.*, vol. 422, p. 213441, 2020, doi: 10.1016/j.ccr.2020.213441.
- S. Huang, X. Zhu, S. Sarkar, and Y. Zhao, "Challenges and opportunities for supercapacitors," *APL Mater.*, vol. 7, no. 10, 2019, doi: 10.1063/1.5116146.
- 47 [7] Y. Zhang *et al.*, "Recent advances and challenges of electrode materials for flexible supercapacitors," *Coord. Chem. Rev.*, vol. 438, p. 213910, 2021, doi: 10.1016/j.ccr.2021.213910.
- 50 [8] S. H. Nagarajarao et al., "Recent Developments in Supercapacitor Electrodes: A Mini

- Review," *ChemEngineering*, vol. 6, no. 1, p. 5, 2022, doi: 10.3390/chemengineering6010005.
- 3 [9] S. Ma *et al.*, "Temperature effect and thermal impact in lithium-ion batteries: A review," *Prog. Nat. Sci. Mater. Int.*, vol. 28, no. 6, pp. 653–666, 2018, doi: 10.1016/j.pnsc.2018.11.002.
- 6 [10] L. Yu and G. Z. Chen, "Redox electrode materials for supercapatteries," *J. Power Sources*, vol. 326, pp. 604–612, 2016, doi: 10.1016/j.jpowsour.2016.04.095.
- 8 [11] Z. Ye, Y. Jiang, L. Li, F. Wu, and R. Chen, *Rational Design of MOF-Based Materials*9 *for Next-Generation Rechargeable Batteries*, vol. 13, no. 1. 2021. doi:
 10.1007/s40820-021-00726-z.
- 11 [12] S. Sundriyal, H. Kaur, S. K. Bhardwaj, S. Mishra, K. H. Kim, and A. Deep, "Metalorganic frameworks and their composites as efficient electrodes for supercapacitor applications," *Coord. Chem. Rev.*, vol. 369, pp. 15–38, 2018, doi: 10.1016/j.ccr.2018.04.018.
- 15 [13] M. Z. Iqbal and U. Aziz, "Supercapattery: Merging of battery-supercapacitor electrodes for hybrid energy storage devices," *J. Energy Storage*, vol. 46, no. December 2021, p. 103823, 2022, doi: 10.1016/j.est.2021.103823.
- 18 [14] A. M. Ullman *et al.*, "Transforming MOFs for Energy Applications Using the Guest@MOF Concept," *Inorg. Chem.*, vol. 55, no. 15, pp. 7233–7249, 2016, doi: 10.1021/acs.inorgchem.6b00909.
- 21 [15] C. Yang, X. Li, L. Yu, X. Liu, J. Yang, and M. Wei, "A new promising Ni-MOF superstructure for high-performance supercapacitors," *Chem. Commun.*, vol. 56, no. 12, pp. 1803–1806, 2020, doi: 10.1039/c9cc09302h.
- Y. R. Lee, J. Kim, and W. S. Ahn, "Synthesis of metal-organic frameworks: A mini review," *Korean J. Chem. Eng.*, vol. 30, no. 9, pp. 1667–1680, 2013, doi: 10.1007/s11814-013-0140-6.
- 27 [17] A. González, E. Goikolea, J. A. Barrena, and R. Mysyk, "Review on supercapacitors: Technologies and materials," *Renew. Sustain. Energy Rev.*, vol. 58, pp. 1189–1206, 2016, doi: 10.1016/j.rser.2015.12.249.
- P. Muhammed, M. Athika, and G. Govindaraj, "Supercapattery performances of nanostructured cerium oxide synthesized using polymer soft-template," *J. Energy Storage*, vol. 28, no. November 2019, p. 101241, 2020, doi: 10.1016/j.est.2020.101241.
- 34 [19] M. Z. Iqbal *et al.*, "Binary composites of strontium oxide/polyaniline for high performance supercapattery devices," *Solid State Ionics*, vol. 347, no. February, p. 115276, 2020, doi: 10.1016/j.ssi.2020.115276.
- B. Ramulu, S. Chandra Sekhar, G. Nagaraju, and J. S. Yu, "Rational design and construction of nickel molybdate nanohybrid composite for high-performance supercapattery," *Appl. Surf. Sci.*, vol. 515, no. November 2019, p. 146023, 2020, doi: 10.1016/j.apsusc.2020.146023.
- M. M. Vadiyar, X. Liu, and Z. Ye, "Highly porous silver dendrites on carbon nanotube wrapped copper cobaltite nano-flowers for boosting energy density and cycle stability of asymmetric supercapattery," *J. Power Sources*, vol. 415, no. January, pp. 154–164, 2019, doi: 10.1016/j.jpowsour.2019.01.053.
- 45 [22] M. Z. Iqbal, M. M. Faisal, S. R. Ali, and A. M. Afzal, "Hydrothermally synthesized zinc phosphate-rGO composites for supercapattery devices," *J. Electroanal. Chem.*, vol. 871, p. 114299, 2020, doi: 10.1016/j.jelechem.2020.114299.
- J. B. Monteiro *et al.*, "MECSE: A CubeSat mission aiming to measure and manipulate the ionospheric plasma layer," *Adv. Astronaut. Sci.*, vol. 163, no. December, pp. 69–81, 2018.

- V. S. Devi, M. Athika, E. Duraisamy, and A. Prasath, "Facile sol-gel derived nanostructured spinel Co 3 O 4 as electrode material for high-performance supercapattery and lithium-ion storage," *J. Energy Storage*, vol. 25, no. July, p. 100815, 2019, doi: 10.1016/j.est.2019.100815.
- Y. Liu, Y. Wang, Y. Chen, C. Wang, and L. Guo, "NiCo-MOF nanosheets wrapping polypyrrole nanotubes for high-performance supercapacitors," *Appl. Surf. Sci.*, vol. 507, no. December 2019, p. 145089, 2020, doi: 10.1016/j.apsusc.2019.145089.
- T. S. Renani, S. M. Khoshfetrat, J. Arjomandi, H. Shi, and S. Khazalpour, "Fabrication and design of new redox active azure A/3D graphene aerogel and conductive trypan blue-nickel MOF nanosheet array electrodes for an asymmetric supercapattery," *J. Mater. Chem. A*, vol. 9, no. 21, pp. 12853–12869, 2021, doi: 10.1039/d1ta02850b.
- 12 [27] H. Wu and Z. Qiu, "Fe3O4@N-porous carbon nano rice/rGO sheet as positive electrode material for a high performance supercapattery," *J. Alloys Compd.*, vol. 879, p. 160264, 2021, doi: 10.1016/j.jallcom.2021.160264.
- [28] T. K. Ghosh, D. L. Singh, V. Mishra, M. K. Sahoo, and G. R. Rao, "Synthesis of Nico-Ldh Using Zif-67 Nanoflake Precursor in Combination with Reduced Graphene Oxide (Rgo) for High Performance Supercapattery Application," SSRN Electron. J., vol. 1, pp. 1–39, 2022, doi: 10.2139/ssrn.4039688.
- 19 [29] B. Akinwolemiwa and G. Z. Chen, "Fundamental consideration for electrochemical engineering of supercapattery," *J. Braz. Chem. Soc.*, vol. 29, no. 5, pp. 960–972, 2018, doi: 10.21577/0103-5053.20180010.
- T. Jin *et al.*, "Microwave synthesis, characterization and catalytic properties of titanium-incorporated ZSM-5 zeolite," *Res. Chem. Intermed.*, vol. 33, no. 6, pp. 501–512, 2007, doi: 10.1163/156856707782565804.
- M. Hartmann, S. Kunz, D. Himsl, O. Tangermann, S. Ernst, and A. Wagener,
 "Adsorptive separation of isobutene and isobutane on Cu3(BTC) 2," *Langmuir*, vol. 24, no. 16, pp. 8634–8642, 2008, doi: 10.1021/la8008656.
- Y. Wang *et al.*, "Ultrathin NiCo-MOF Nanosheets for High-Performance
 Supercapacitor Electrodes," *ACS Appl. Energy Mater.*, vol. 2, no. 3, pp. 2063–2071,
 2019, doi: 10.1021/acsaem.8b02128.
- H. Daglar *et al.*, "Effect of Metal–Organic Framework (MOF) Database Selection on the Assessment of Gas Storage and Separation Potentials of MOFs," *Angew. Chemie*, vol. 133, no. 14, pp. 7907–7916, 2021, doi: 10.1002/ange.202015250.
- 34 [34] M. Bonneau, C. Lavenn, P. Ginet, K. I. Otake, and S. Kitagawa, "Upscale synthesis of a binary pillared layered MOF for hydrocarbon gas storage and separation," *Green Chem.*, vol. 22, no. 3, pp. 718–724, 2020, doi: 10.1039/c9gc03561c.
- 37 [35] S. Chen, Y. Li, and L. Mi, "Porous carbon derived from metal organic framework for gas storage and separation: The size effect," *Inorg. Chem. Commun.*, vol. 118, no. April, p. 107999, 2020, doi: 10.1016/j.inoche.2020.107999.
- 40 [36] S. Dawood, S. Shaji, G. Pathiraja, Y. Mo, and H. Rathnayake, "Molecular magnetism in nanodomains of isoreticular MIL-88(Fe)-MOFs," *Phys. Chem. Chem. Phys.*, vol. 23, no. 38, pp. 21677–21689, 2021, doi: 10.1039/d1cp03122h.
- 43 [37] S. Kim *et al.*, "Hybrids of Pd Nanoparticles and Metal-Organic Frameworks for Enhanced Magnetism," *J. Phys. Chem. Lett.*, vol. 12, no. 19, pp. 4742–4748, 2021, doi: 10.1021/acs.jpclett.1c01108.
- 46 [38] S. I. Vasylevskyy *et al.*, "1,2,4-triazolyl-carboxylate-based MOFs incorporating triangular Cu(II)-hydroxo clusters: Topological metamorphosis and magnetism," *Inorg. Chem.*, vol. 53, no. 7, pp. 3642–3654, 2014, doi: 10.1021/ic403148f.
- [39] S. F. Li *et al.*, "Different Phenomena in Magnetic/Electrical Properties of Co(II) and
 Ni(II) Isomorphous MOFs," *ACS Omega*, vol. 6, no. 13, pp. 9213–9221, 2021, doi:

- 1 10.1021/acsomega.1c00574.
- H. Yurtseven and E. Kilit Dogan, "Magnetic, thermal and ferroelectric properties of MOFs (MHyM, M = Fe, Mn) close to phase transitions," *J. Magn. Magn. Mater.*, vol. 540, no. April, 2021, doi: 10.1016/j.jmmm.2021.168489.
- [41] M. N. Ahamad, M. Shahid, M. Ahmad, and F. Sama, "Cu(II) MOFs Based on
 Bipyridyls: Topology, Magnetism, and Exploring Sensing Ability toward Multiple
 Nitroaromatic Explosives," ACS Omega, vol. 4, no. 4, pp. 7738–7749, 2019, doi:
 10.1021/acsomega.9b00715.
- 9 [42] A. Herbst, A. Khutia, and C. Janiak, "Brønsted instead of lewis acidity in functionalized MIL-101Cr MOFs for efficient heterogeneous (nano-MOF) catalysis in the condensation reaction of aldehydes with alcohols," *Inorg. Chem.*, vol. 53, no. 14, pp. 7319–7333, 2014, doi: 10.1021/ic5006456.
- Y. B. N. Tran, P. T. K. Nguyen, Q. T. Luong, and K. D. Nguyen, "Series of M-MOF-184 (M = Mg, Co, Ni, Zn, Cu, Fe) Metal-Organic Frameworks for Catalysis
 Cycloaddition of CO2," *Inorg. Chem.*, vol. 59, no. 22, pp. 16747–16759, 2020, doi: 10.1021/acs.inorgchem.0c02807.
- 17 [44] H. Li *et al.*, "Postsynthesis Strategy of Functional Zn-MOF Sensors for the Detection
 18 of ClO-and DPA," *Inorg. Chem.*, vol. 60, no. 4, pp. 2590–2597, 2021, doi:
 10.1021/acs.inorgchem.0c03468.
- 20 [45] B. Li *et al.*, "Rational design, synthesis, and applications of carbon dots@metal— 21 organic frameworks (CD@MOF) based sensors," *TrAC - Trends Anal. Chem.*, vol. 135, p. 116163, 2021, doi: 10.1016/j.trac.2020.116163.
- [46] O. Yassine, O. Shekhah, A. H. Assen, Y. Belmabkhout, K. N. Salama, and M.
 Eddaoudi, "H 2 S Sensors: Fumarate-Based fcu-MOF Thin Film Grown on a
 Capacitive Interdigitated Electrode," *Angew. Chemie*, vol. 128, no. 51, pp. 16111–
 16115, 2016, doi: 10.1002/ange.201608780.
- J. Schnabel, R. Ettlinger, and H. Bunzen, "Zn-MOF-74 as pH-Responsive Drug-Delivery System of Arsenic Trioxide," *ChemNanoMat*, vol. 6, no. 8, pp. 1229–1236, 2020, doi: 10.1002/cnma.202000221.
- [48] J. Hu, Y. Chen, H. Zhang, and Z. Chen, "Controlled syntheses of Mg-MOF-74 nanorods for drug delivery," *J. Solid State Chem.*, vol. 294, no. October 2020, p. 121853, 2021, doi: 10.1016/j.jssc.2020.121853.
- I. Abánades Lázaro, S. Abánades Lázaro, and R. S. Forgan, "Enhancing anticancer cytotoxicity through bimodal drug delivery from ultrasmall Zr MOF nanoparticles,"
 Chem. Commun., vol. 54, no. 22, pp. 2792–2795, 2018, doi: 10.1039/c7cc09739e.
- Q. L. Guan *et al.*, "Bismuth-MOF based on tetraphenylethylene derivative as a luminescent sensor with turn-off/on for application of Fe3+ detection in serum and bioimaging, as well as emissive spectra analysis by TRES," *Sensors Actuators, B Chem.*, vol. 325, no. July, p. 128767, 2020, doi: 10.1016/j.snb.2020.128767.
- S. Bhowal and A. Ghosh, "Highly selective fluorescent turn-on-off sensing of OH–, Al3+and Fe3+ions by tuning ESIPT in metal organic frameworks and mitochondria targeted bio-imaging," *RSC Adv.*, vol. 11, no. 45, pp. 27787–27800, 2021, doi: 10.1039/d1ra03078g.
- 44 [52] A. Singh *et al.*, "Unraveling the Effect on Luminescent Properties by Postsynthetic Covalent and Noncovalent Grafting of gfp Chromophore Analogues in Nanoscale MOF-808," *Inorg. Chem.*, vol. 59, no. 12, pp. 8251–8258, 2020, doi: 10.1021/acs.inorgchem.0c00625.
- 48 [53] C. Qu *et al.*, "Nickel-based pillared MOFs for high-performance supercapacitors:
 49 Design, synthesis and stability study," *Nano Energy*, vol. 26, pp. 66–73, 2016, doi:
 50 10.1016/j.nanoen.2016.04.003.

- 1 [54] H. Xia, J. Zhang, Z. Yang, S. Guo, S. Guo, and Q. Xu, "2D MOF nanoflake-assembled spherical microstructures for enhanced supercapacitor and electrocatalysis performances," *Nano-Micro Lett.*, vol. 9, no. 4, pp. 1–11, 2017, doi: 10.1007/s40820-017-0144-6.
- [55] I. A. Khan, A. Badshah, M. A. Nadeem, N. Haider, and M. A. Nadeem, "A copper based metal-organic framework as single source for the synthesis of electrode materials for high-performance super capacitors and glucose sensing applications," *Int. J. Hydrogen Energy*, vol. 39, no. 34, pp. 19609–19620, 2014, doi: 10.1016/j.ijhydene.2014.09.106.
- 10 [56] N. Liu, X. Liu, and J. Pan, "A new rapid synthesis of hexagonal prism Zn-MOF as a precursor at room temperature for energy storage through pre-ionization strategy," *J. Colloid Interface Sci.*, vol. 606, pp. 1364–1373, 2022, doi: 10.1016/j.jcis.2021.08.105.
- 13 [57] Q. B. Le *et al.*, "Electrochemical performance of composites made of rGO with Zn-14 MOF and PANI as electrodes for supercapacitors," *Electrochim. Acta*, vol. 367, p. 15 137563, 2021, doi: 10.1016/j.electacta.2020.137563.
- [58] L. Zhang, H. Bin Wu, S. Madhavi, H. H. Hng, and X. W. Lou, "Formation of Fe 2O 3 microboxes with hierarchical shell structures from metal-organic frameworks and their lithium storage properties," *J. Am. Chem. Soc.*, vol. 134, no. 42, pp. 17388–17391, 2012, doi: 10.1021/ja307475c.
- Y. Sun *et al.*, "A green and template-free synthesis process of superior carbon material with ellipsoidal structure as enhanced material for supercapacitors," *J. Power Sources*, vol. 405, no. July, pp. 80–88, 2018, doi: 10.1016/j.jpowsour.2018.10.034.
- 23 [60] S. Osman, R. A. Senthil, J. Pan, and W. Li, "Highly activated porous carbon with 3D microspherical structure and hierarchical pores as greatly enhanced cathode material for high-performance supercapacitors," *J. Power Sources*, vol. 391, no. April, pp. 162–169, 2018, doi: 10.1016/j.jpowsour.2018.04.081.
- V. Yang, R. A. Senthil, J. Pan, T. R. Kumar, Y. Sun, and X. Liu, "Hierarchical porous carbon derived from jujube fruits as sustainable and ultrahigh capacitance material for advanced supercapacitors," *J. Colloid Interface Sci.*, 2020, doi: 10.1016/j.jcis.2020.06.080.
- J. Xiao, N. A. Chernova, and M. S. Whittingham, "Layered mixed transition metal oxide cathodes with reduced cobalt content for lithium ion batteries," *Chem. Mater.*, vol. 20, no. 24, pp. 7454–7464, 2008, doi: 10.1021/cm802316d.
- H. Kim *et al.*, "Stoichiometric Layered Potassium Transition Metal Oxide for Rechargeable Potassium Batteries," *Chem. Mater.*, vol. 30, no. 18, pp. 6532–6539, 2018, doi: 10.1021/acs.chemmater.8b03228.
- C. Luo, A. Langrock, X. Fan, Y. Liang, and C. Wang, "P2-type transition metal oxides for high performance Na-ion battery cathodes," *J. Mater. Chem. A*, vol. 5, no. 34, pp. 18214–18220, 2017, doi: 10.1039/c7ta04515h.
- 40 [65] Y. Wang and Y. C. Lu, "Nonaqueous Lithium—Oxygen batteries: Reaction mechanism and critical open questions," *Energy Storage Mater.*, vol. 28, no. March, pp. 235–246, 2020, doi: 10.1016/j.ensm.2020.03.007.
- [66] H. Yuan *et al.*, "Efficient Activation of Li2S by Transition Metal Phosphides
 Nanoparticles for Highly Stable Lithium-Sulfur Batteries," *ACS Energy Lett.*, vol. 2,
 no. 7, pp. 1711–1719, 2017, doi: 10.1021/acsenergylett.7b00465.
- 46 [67] X. He *et al.*, "In Situ Investigations on the Structural and Morphological Changes of
 47 Metal Phosphides as Anode Materials in Lithium-Ion Batteries," *Adv. Mater.* 48 *Interfaces*, vol. 4, no. 7, pp. 1–9, 2017, doi: 10.1002/admi.201601047.
- Z. Huang, H. Hou, C. Wang, S. Li, Y. Zhang, and X. Ji, "Molybdenum Phosphide: A
 Conversion-type Anode for Ultralong-Life Sodium-Ion Batteries," *Chem. Mater.*, vol.

- 29, no. 17, pp. 7313–7322, 2017, doi: 10.1021/acs.chemmater.7b02193.
- Y. Liu, T. Mastumura, Y. Ono, N. Imanishi, A. Hirano, and Y. Takeda,
 "Electrochemical behavior of the composite anodes consisting of carbonaceous
 materials and lithium transition-metal nitrides for lithium-ion batteries," *Solid State Ionics*, vol. 179, no. 35–36, pp. 2069–2073, 2008, doi: 10.1016/j.ssi.2008.07.007.
- [70] Z. Ma, Z. Li, Y. Zeng, P. Li, and H. Zhang, "High electrochemical performance of Γ" FeN thin film electrode for lithium ion batteries," *J. Power Sources*, vol. 423, no.
 March, pp. 159–165, 2019, doi: 10.1016/j.jpowsour.2019.03.074.
- 9 [71] Q. Zhao, X. Liu, S. Stalin, K. Khan, and L. A. Archer, "Solid-state polymer electrolytes with in-built fast interfacial transport for secondary lithium batteries," *Nat. Energy*, vol. 4, no. 5, pp. 365–373, 2019, doi: 10.1038/s41560-019-0349-7.
- 12 [72] S. Saffirio, M. Falco, G. B. Appetecchi, F. Smeacetto, and C. Gerbaldi, "Li1.4Al0.4Ge0.4Ti1.4(PO4)3 promising NASICON-structured glass-ceramic 14 electrolyte for all-solid-state Li-based batteries: Unravelling the effect of diboron 15 trioxide," *J. Eur. Ceram. Soc.*, vol. 42, no. 3, pp. 1023–1032, 2022, doi: 10.1016/j.jeurceramsoc.2021.11.014.
- 17 [73] L. Liang *et al.*, "Construction and Operating Mechanism of High-Rate Mo-Doped Na3V2(PO4)3@C Nanowires toward Practicable Wide-Temperature-Tolerance Na-Ion and Hybrid Li/Na-Ion Batteries," *Adv. Energy Mater.*, vol. 11, no. 21, pp. 1–17, 2021, doi: 10.1002/aenm.202100287.
- 21 [74] A. Kamiyama *et al.*, "MgO-Template Synthesis of Extremely High Capacity Hard Carbon for Na-Ion Battery," *Angew. Chemie Int. Ed.*, vol. 60, no. 10, pp. 5114–5120, 2021, doi: 10.1002/anie.202013951.
- Q. Li, S. Zhu, and Y. Lu, "3D Porous Cu Current Collector/Li-Metal Composite
 Anode for Stable Lithium-Metal Batteries," *Adv. Funct. Mater.*, vol. 27, no. 18, 2017, doi: 10.1002/adfm.201606422.
- [76] C. Jin *et al.*, "3D lithium metal embedded within lithiophilic porous matrix for stable lithium metal batteries," *Nano Energy*, vol. 37, pp. 177–186, 2017, doi: 10.1016/j.nanoen.2017.05.015.
- [77] S. H. Lee, J. Y. Hwang, S. J. Park, G. T. Park, and Y. K. Sun, "Adiponitrile (C6H8N2): A New Bi-Functional Additive for High-Performance Li-Metal Batteries,"
 Adv. Funct. Mater., vol. 29, no. 30, pp. 1–9, 2019, doi: 10.1002/adfm.201902496.
- R. Xiong, L. Li, and J. Tian, "Towards a smarter battery management system: A critical review on battery state of health monitoring methods," *J. Power Sources*, vol. 405, no. 5, pp. 18–29, 2018, doi: 10.1016/j.jpowsour.2018.10.019.
- 36 [79] X. I. A. HUANG *et al.*, "Cyclic voltammetry in Lithium-sulfur battery challenges and opportunities," *Energy Technol.*, vol. 7, Aug. 2019, doi: 10.1002/ente.201801001.
- T. S. Mathis, N. Kurra, X. Wang, D. Pinto, P. Simon, and Y. Gogotsi, "Energy Storage Data Reporting in Perspective—Guidelines for Interpreting the Performance of Electrochemical Energy Storage Systems," *Adv. Energy Mater.*, vol. 9, no. 39, pp. 1–13, 2019, doi: 10.1002/aenm.201902007.
- F. Cheng, X. Yang, S. Zhang, and W. Lu, "Boosting the supercapacitor performances of activated carbon with carbon nanomaterials," *J. Power Sources*, vol. 450, no. November 2019, p. 227678, 2020, doi: 10.1016/j.jpowsour.2019.227678.
- 45 [82] T. Liu, F. Zhang, Y. Song, and Y. Li, "Revitalizing carbon supercapacitor electrodes with hierarchical porous structures," *J. Mater. Chem. A*, vol. 5, no. 34, pp. 17705–17733, 2017, doi: 10.1039/c7ta05646j.
- 48 [83] S. Unknown, P. Chand, and A. Joshi, "Biomass derived carbon for supercapacitor applications: Review," *J. Energy Storage*, vol. 39, no. April, p. 102646, 2021, doi: 10.1016/j.est.2021.102646.

- 2 Z. Yang *et al.*, "Free-standing PEDOT/polyaniline conductive polymer hydrogel for flexible solid-state supercapacitors," *Electrochim. Acta*, vol. 322, p. 134769, 2019, doi: 10.1016/j.electacta.2019.134769.
- 4 [85] B. S. Yin, S. W. Zhang, K. Ke, and Z. B. Wang, "Advanced deformable all-in-one hydrogel supercapacitor based on conducting polymer: Toward integrated mechanical and capacitive performance," *J. Alloys Compd.*, vol. 805, pp. 1044–1051, 2019, doi: 10.1016/j.jallcom.2019.07.144.
- 8 [86] V. Augustyn, "Tuning the interlayer of transition metal oxides for electrochemical energy storage," *J. Mater. Res.*, vol. 32, no. 1, pp. 2–15, 2017, doi: 10.1557/imr.2016.337.
- 11 [87] A. Das, B. Raj, M. Mohapatra, S. M. Andersen, and S. Basu, "Performance and future directions of transition metal sulfide-based electrode materials towards supercapacitor/supercapattery," *Wiley Interdiscip. Rev. Energy Environ.*, vol. 11, no. 1, 2022, doi: 10.1002/wene.414.
- [88] L. Liu, H. Zhao, and Y. Lei, "Review on Nanoarchitectured Current Collectors for Pseudocapacitors," *Small Methods*, vol. 3, no. 8, pp. 1–25, 2019, doi: 10.1002/smtd.201800341.
- 18 [89] M. Z. Iqbal *et al.*, "Copper doped cobalt-manganese phosphate ternary composites for high-performance supercapattery devices," *J. Energy Storage*, vol. 35, no. November 20 2020, p. 102307, 2021, doi: 10.1016/j.est.2021.102307.
- 21 [90] M. Z. Iqbal, J. Khan, A. M. Afzal, and S. Aftab, "Exploring the synergetic electrochemical performance of cobalt sulfide/cobalt phosphate composites for supercapattery devices with high-energy and rate capability," *Electrochim. Acta*, vol. 384, p. 138358, 2021, doi: 10.1016/j.electacta.2021.138358.
- P. V. Shinde, N. M. Shinde, J. M. Yun, R. S. Mane, and K. H. Kim, "Facile Chemical Synthesis and Potential Supercapattery Energy Storage Application of Hydrangea-type Bi2MoO6," *ACS Omega*, vol. 4, no. 6, pp. 11093–11102, 2019, doi: 10.1021/acsomega.9b00522.
- [92] K. Venkata, G. Raghavendra, K. Madhusudana, and N. T. U. Kumar, "Hydrothermal synthesis of CuS / CoS nano composite as an efficient electrode for the supercapattery applications," *J. Energy Storage*, vol. 40, no. May, p. 102749, 2021, doi: 10.1016/j.est.2021.102749.
- S. Liang, H. Wang, Y. Li, H. Qin, Z. Luo, and L. Chen, "Applied Surface Science
 Ternary synergistic transition metal oxalate 2D porous thin sheets assembled by 3D
 nanoflake array with high performance for supercapattery," *Appl. Surf. Sci.*, vol. 567,
 no. August, p. 150809, 2021, doi: 10.1016/j.apsusc.2021.150809.
- M. Roman *et al.*, "Exalted redox frameworks of Cu-MOF/polyaniline/RGO based composite electrodes by integrating silver nanoparticles as a catalytic agent for superior energy featured supercapatteries," *Electrochim. Acta*, vol. 400, p. 139489, 2021, doi: 10.1016/j.electacta.2021.139489.
- [95] S. Anantharaj, S. R. Ede, K. Sakthikumar, K. Karthick, S. Mishra, and S. Kundu,
 "Recent Trends and Perspectives in Electrochemical Water Splitting with an Emphasis on Sulfide, Selenide, and Phosphide Catalysts of Fe, Co, and Ni: A Review," ACS
 Catal., vol. 6, no. 12, pp. 8069–8097, 2016, doi: 10.1021/acscatal.6b02479.
- J. J. William, I. M. Babu, and G. Muralidharan, "Spongy structured a -Ni (OH) 2:
 Facile and rapid synthesis for supercapattery applications," *Mater. Lett.*, vol. 238, pp. 35–37, 2019, doi: 10.1016/j.matlet.2018.11.136.
- 48 [97] L. Gurusamy *et al.*, "Enhanced performance of charge storage supercapattery by dominant oxygen deficiency in crystal defects of 2-D MoO3-x nanoplates," *Appl. Surf.* 50 *Sci.*, vol. 541, no. November 2020, p. 148676, 2021, doi:

1 10.1016/j.apsusc.2020.148676.

29

30

- [98] I. M. Babu, J. J. William, and G. Muralidharan, "Hierarchical β -Co (OH) 2 / CoO nanosheets: an additive-free synthesis approach for supercapattery applications,"
 2019.
- [99] G. Liu *et al.*, "Constructing 3D honeycomb-like CoMn2O4 nanoarchitecture on nitrogen-doped graphene coating Ni foam as flexible battery-type electrodes for advanced supercapattery," *Int. J. Hydrogen Energy*, vol. 46, no. 73, pp. 36314–36322, 2021, doi: 10.1016/j.ijhydene.2021.08.159.
- 9 [100] B. C. Kim *et al.*, "Efficient supercapattery behavior of mesoporous hydrous and anhydrous cobalt molybdate nanostructures," *J. Alloys Compd.*, vol. 789, pp. 256–265, 2019, doi: 10.1016/j.jallcom.2019.03.033.
- 12 [101] Y. Chen, W. Yang, S. Gao, C. Sun, and Q. Li, "Synthesis of Bi2MoO6 Nanosheets with Rich Oxygen Vacancies by Postsynthesis Etching Treatment for Enhanced Photocatalytic Performance," *ACS Appl. Nano Mater.*, vol. 1, no. 7, pp. 3565–3578, Jul. 2018, doi: 10.1021/acsanm.8b00719.
- 16 [102] Q. Lu, Y. Chen, W. Li, J. G. Chen, J. Q. Xiao, and F. Jiao, "Ordered mesoporous nickel cobaltite spinel with ultra-high supercapacitance," *J. Mater. Chem. A*, vol. 1, no. 6, pp. 2331–2336, 2013, doi: 10.1039/c2ta00921h.
- [103] M. Zhu, D. Meng, C. Wang, and G. Diao, "Facile fabrication of hierarchically porous
 CuFe2O4 nanospheres with enhanced capacitance property.," ACS Appl. Mater.
 Interfaces, vol. 5, no. 13, pp. 6030–6037, Jul. 2013, doi: 10.1021/am4007353.
- [104] M. Z. Iqbal, S. S. H. Sana Zakar, and M. Alzaid, "Superior performance of cobalt oxide/carbon composite for solid-state supercapattery devices," *Phys. B Condens. Matter*, vol. 603, no. November 2020, p. 412561, 2021, doi: 10.1016/j.physb.2020.412561.
- [105] E. S. Agudosi, E. C. Abdullah, A. Numan, N. M. Mubarak, S. R. Aid, and R. B. Vilau,
 "Fabrication of 3D binder free graphene NiO electrode for highly stable
 supercapattery," *Sci. Rep.*, pp. 1–13, 2020, doi: 10.1038/s41598-020-68067-2.
 - [106] J. Iqbal *et al.*, "Facile synthesis of ternary nanocomposite of polypyrrole incorporated with cobalt oxide and silver nanoparticles for high performance supercapattery," *Electrochim. Acta*, vol. 348, p. 136313, 2020, doi: 10.1016/j.electacta.2020.136313.
- [107] K. Chhetri *et al.*, "Hollow Carbon Nanofibers with Inside-outside Decoration of Bimetallic MOF Derived Ni-Fe Phosphides as Electrode Materials for Asymmetric Supercapacitors," *Chem. Eng. J.*, vol. 450, no. P4, p. 138363, 2022, doi: 10.1016/j.cej.2022.138363.
- 36 [108] S. Alam and M. Z. Iqbal, "Nickel-manganese phosphate: An efficient battery-grade electrode for supercapattery devices," *Ceram. Int.*, vol. 47, no. 8, pp. 11220–11230, 2021, doi: 10.1016/j.ceramint.2020.12.247.
- [109] M. Z. Iqbal, J. Khan, S. Siddique, A. M. Afzal, and S. Aftab, "Optimizing electrochemical performance of sonochemically and hydrothermally synthesized cobalt phosphate for supercapattery devices," *Int. J. Hydrogen Energy*, vol. 46, no. 29, pp. 15807–15819, 2021, doi: 10.1016/j.ijhydene.2021.02.077.
- [110] H. Shao, N. Padmanathan, D. McNulty, C. O'Dwyer, and K. M. Razeeb,
 "Supercapattery Based on Binder-Free Co3(PO4)2·8H2O Multilayer
 Nano/Microflakes on Nickel Foam," ACS Appl. Mater. Interfaces, vol. 8, no. 42, pp. 28592–28598, 2016, doi: 10.1021/acsami.6b08354.
- 47 [111] S. Alam, M. Z. Iqbal, and J. Khan, "Green synthesis of nickel-manganese/polyaniline-based ternary composites for high-performance supercapattery devices," *Int. J. Energy* 49 *Res.*, vol. 45, no. 7, pp. 11109–11122, 2021, doi: 10.1002/er.6593.
- 50 [112] M. Z. Iqbal, J. Khan, H. T. A. Awan, M. Alzaid, A. M. Afzal, and S. Aftab, "Cobalt-

- manganese-zinc ternary phosphate for high performance supercapattery devices," *Dalt. Trans.*, vol. 49, no. 46, pp. 16715–16727, 2020, doi: 10.1039/d0dt03313h.
- 3 [113] M. Alzaid, M. Z. Iqbal, S. Siddique, and N. M. A. Hadia, "Exploring the electrochemical performance of copper-doped cobalt-manganese phosphates for potential supercapattery applications," *RSC Adv.*, vol. 11, no. 45, pp. 28042–28051, 2021, doi: 10.1039/d0ra09952j.

8 9

- [114] H. Shao, N. Padmanathan, D. McNulty, C. O'Dwyer, and K. M. Razeeb, "Cobalt phosphate-based supercapattery as alternative power source for implantable medical devices," *ACS Appl. Energy Mater.*, vol. 2, no. 1, pp. 569–578, 2019, doi: 10.1021/acsaem.8b01612.
- 11 [115] S. Surendran, S. Shanmugapriya, A. Sivanantham, S. Shanmugam, and R. Kalai Selvan, "Electrospun Carbon Nanofibers Encapsulated with NiCoP: A Multifunctional Electrode for Supercapattery and Oxygen Reduction, Oxygen Evolution, and Hydrogen Evolution Reactions," *Adv. Energy Mater.*, vol. 8, no. 20, pp. 1–18, 2018, doi: 10.1002/aenm.201800555.
- [116] S. Vinoth, W. J. Ong, and A. Pandikumar, "Sulfur-doped graphitic carbon nitride incorporated bismuth oxychloride/Cobalt based type-II heterojunction as a highly stable material for photoelectrochemical water splitting," *J. Colloid Interface Sci.*, vol. 591, pp. 85–95, 2021, doi: 10.1016/j.jcis.2021.01.104.
- [117] S. Surendran and R. K. Selvan, "Growth and Characterization of 3D Flower-Like β-NiS on Carbon Cloth: A Dexterous and Flexible Multifunctional Electrode for Supercapattery and Water-Splitting Applications," *Adv. Mater. Interfaces*, vol. 5, no. 4, pp. 1–12, 2018, doi: 10.1002/admi.201701056.
- [118] S. Surendran, S. Shanmugapriya, and H. Ramasamy, "Applied Surface Science
 Hydrothermal deposition of CoS nanostructures and its multifunctional applications in
 supercapattery and water electrolyzer," *Appl. Surf. Sci.*, vol. 494, no. July, pp. 916–
 928, 2019, doi: 10.1016/j.apsusc.2019.07.162.
- 28 [119] X. Wang *et al.*, "Plasma-induced on-surface sulfur vacancies in NiCo2S4 enhance the energy storage performance of supercapatteries," *J. Mater. Chem. A*, vol. 8, no. 18, pp. 9278–9291, 2020, doi: 10.1039/D0TA01991G.
- [120] K. Nasrin, K. Subramani, M. Karnan, and M. Sathish, "MnCo2S4 MXene: A novel hybrid electrode material for high performance long-life asymmetric supercapattery,"
 J. Colloid Interface Sci., vol. 600, pp. 264–277, 2021, doi: 10.1016/j.jcis.2021.05.037.
- 34 [121] N. M. Shinde *et al.*, "Ultra-rapid chemical synthesis of mesoporous Bi2O3 microsponge-balls for supercapattery applications," *Electrochim. Acta*, vol. 296, pp. 308–316, 2019, doi: 10.1016/j.electacta.2018.11.044.
- 37 [122] A. Numan *et al.*, "Facile sonochemical synthesis of 2D porous Co3O4 nanoflake for supercapattery," *J. Alloys Compd.*, vol. 819, p. 153019, 2020, doi: 10.1016/j.jallcom.2019.153019.
- Il [123] J. Iqbal *et al.*, "Ternary nanocomposite of cobalt oxide nanograins and silver nanoparticles grown on reduced graphene oxide conducting platform for high-performance supercapattery electrode material," *J. Alloys Compd.*, vol. 821, p. 153452, 2020, doi: 10.1016/j.jallcom.2019.153452.
- [124] S. B. Bandgar, M. M. Vadiyar, C. L. Jambhale, Z. Ye, J. H. Kim, and S. S. Kolekar,
 "Construction of dual metal ferrite-based core-shell nanostructures as low-cost
 multimetal electrode for boosting energy density of flexible asymmetric
 supercapattery," *J. Energy Storage*, vol. 36, no. December 2020, p. 102379, 2021, doi: 10.1016/j.est.2021.102379.
- [125] M. M. Ndipingwi *et al.*, "Orthorhombic Nanostructured Li2MnSiO4/Al2O3
 Supercapattery Electrode with Efficient Lithium-Ion Migratory Pathway," *Batter*.

- 1 Supercaps, vol. 1, no. 6, pp. 223–235, 2018, doi: 10.1002/batt.201800045.
- 2 [126] L. Yu and G. Z. Chen, "High energy supercapattery with an ionic liquid solution of LiClO4," *Faraday Discuss.*, vol. 190, pp. 231–240, 2016, doi: 10.1039/c5fd00232j.
- NiO–In2O3 microflower (3D)/ nanorod (1D) hetero-architecture as a supercapattery electrode with excellent cyclic stability," *J. Mater. Chem. A*, vol. 4, no. 13, pp. 4820–4830, 2016, doi: 10.1039/C5TA10407F.
- 8 [128] S. Raj, P. Kar, and P. Roy, "Facile synthesis of flower-like morphology
 9 Cu0.27Co2.73O4 for a high-performance supercapattery with extraordinary cycling
 10 stability," *Chem. Commun.*, vol. 54, no. 87, pp. 12400–12403, 2018, doi:
 11 10.1039/c8cc04625e.
- 12 [129] S. Archana, M. Athika, and P. Elumalai, "Supercapattery and full-cell lithium-ion battery performances of a [Ni(Schiff base)]-derived Ni/NiO/nitrogen-doped carbon heterostructure," *New J. Chem.*, vol. 44, no. 29, pp. 12452–12464, 2020, doi: 10.1039/d0nj01602k.
- 16 [130] "Accepted Article", doi: 10.1002/ente.201900387.
- 17 [131] B. Saravanakumar, X. Wang, W. Zhang, L. Xing, and W. Li, "Holey Two Dimensional Manganese Cobalt Oxide Nanosheets as a High-performance Electrode for Supercapattery," *Chem. Eng. J.*, 2019, doi: 10.1016/j.cej.2019.05.080.
- 20 [132] B. Huang *et al.*, "Two-dimensional porous cobalt—nickel tungstate thin sheets for high performance supercapattery," *Energy Storage Mater.*, 2020, doi: 10.1016/j.ensm.2020.07.014.
- [133] D. J. Tarimo, K. O. Oyedotun, A. A. Mirghni, B. Mutuma, N. F. Sylla, and P.
 Murovhi, "ScienceDirect Enhanced electrochemical performance of supercapattery derived from sulphur-reduced graphene oxide / cobalt oxide composite and activated carbon from peanut shells," *Int. J. Hydrogen Energy*, no. xxxx, 2020, doi: 10.1016/j.ijhydene.2020.09.142.
- 28 [134] S. Seenivasan *et al.*, "Boosting Pseudocapacitive Behavior of Supercapattery
 29 Electrodes by Incorporating a Schottky Junction for Ultrahigh Energy Density," *Nano-*30 *Micro Lett.*, vol. 15, no. 1, p. 62, 2023, doi: 10.1007/s40820-023-01016-6.
- [135] T. Kavinkumar, S. Seenivasan, A. T. Sivagurunathan, Y. Kwon, and D.-H. Kim,
 "Three-Dimensional Hierarchical Core/shell Electrodes Using Highly Conformal TiO2
 and Co3O4 Thin Films for High-Performance Supercapattery Devices," ACS Appl.
 Mater. Interfaces, vol. 13, no. 24, pp. 29058–29069, Jun. 2021, doi:
 10.1021/acsami.1c04572.
- [136] P. Supercapattery, J. Iqbal, A. Numan, M. O. Ansari, and R. Jafer, "Cobalt Oxide
 Nanograins and Silver Nanoparticles Decorated Fibrous Polyaniline Nanocomposite as
 Battery-Type Electrode for High," pp. 1–19, 2020.
- 39 [137] M. Z. Iqbal *et al.*, "Strontium phosphide-polyaniline composites for high performance supercapattery devices," *Ceram. Int.*, vol. 46, no. 8, pp. 10203–10214, 2020, doi: 10.1016/j.ceramint.2020.01.012.
- 42 [138] R. Justinabraham *et al.*, "Synthesis of porous g-C3N4 doped vanadyl phosphate for supercapattery application," *J. Energy Storage*, vol. 40, no. May, p. 102786, 2021, doi: 10.1016/j.est.2021.102786.
- [139] S. Surendran, S. Shanmugapriya, S. Shanmugam, L. Vasylechko, and R. Kalai Selvan,
 "Interweaved Nickel Phosphide Sponge as an Electrode for Flexible Supercapattery
 and Water Splitting Applications," *ACS Appl. Energy Mater.*, vol. 1, no. 1, pp. 78–92,
 2018, doi: 10.1021/acsaem.7b00006.
- [140] F. Alam, M. Zahir, S. Alam, and N. Alhassan, "Binary composites of sonochemically synthesized cobalt phosphates / polyaniline for supercapattery devices," *J. Energy*

- 1 Storage, vol. 42, no. August, p. 103150, 2021, doi: 10.1016/j.est.2021.103150.
- 2 [141] R. Asadi, A. M. Zardkhoshoui, S. N. Azizi, and S. S. Hosseiny Davarani, "Designing an Advanced Supercapattery Based on CuCo2S4@Ni-Mo-S Nanosheet Arrays,"

 4 ChemElectroChem, vol. 6, no. 24, pp. 5984–5992, 2019, doi: 10.1002/celc.201901385.
- [142] J. Lin *et al.*, "Designing and constructing core-shell NiCo2S4@Ni3S2 on Ni foam by facile one-step strategy as advanced battery-type electrodes for supercapattery," *J. Colloid Interface Sci.*, 2018, doi: 10.1016/j.jcis.2018.10.072.
- 8 [143] J. Lin *et al.*, "Rational constructing free-standing Se doped nickel-cobalt sulfides 9 nanotubes as battery-type electrode for high-performance supercapattery," *J. Power* 10 *Sources*, vol. 407, pp. 6–13, 2018, doi: 11 https://doi.org/10.1016/j.jpowsour.2018.10.046.
- 12 [144] Q. Hu *et al.*, "Core-shell MnO 2 @ CoS nanosheets with oxygen vacancies for high-13 performance supercapattery," *J. Power Sources*, vol. 446, no. July 2019, p. 227335, 14 2020, doi: 10.1016/j.jpowsour.2019.227335.
- 15 [145] C. Z. Kang, F. S. Omar, S. Gunalan, K. Ramesh, and S. Ramesh, "Coral-like structured nickel sulfide-cobalt sulfide binder-free electrode for supercapattery," pp. 3621–3630, 2020.
- 18 [146] H. W. Lee, N. M. Shinde, and K. H. Kim, "High energy and power density of self-19 grown CuS @ Cu 2 O core-shell supercapattery positrode," 2019.
- [147] J. Jiang *et al.*, "An Amorphous Crystalline Nanosheet Arrays Structure for Ultrahigh
 Electrochemical Performance Supercapattery," vol. 2102565, pp. 1–10, 2021, doi:
 10.1002/smll.202102565.
- 23 [148] N. Stock and S. Biswas, "Synthesis of metal-organic frameworks (MOFs): Routes to various MOF topologies, morphologies, and composites," *Chem. Rev.*, vol. 112, no. 2, pp. 933–969, 2012, doi: 10.1021/cr200304e.
- [149] M. Yu, L. Zhang, X. He, H. Yu, J. Han, and M. Wu, "3D interconnected porous carbons from MOF-5 for supercapacitors," *Mater. Lett.*, vol. 172, pp. 81–84, 2016, doi: 10.1016/j.matlet.2016.02.144.
- [150] X. Cai, J. Lin, and M. Pang, "Facile Synthesis of Highly Uniform Fe-MIL-88B
 Particles," *Cryst. Growth Des.*, vol. 16, no. 7, pp. 3565–3568, 2016, doi: 10.1021/acs.cgd.6b00313.
- [151] S. Zuluaga *et al.*, "Understanding and controlling water stability of MOF-74," *J. Mater. Chem. A*, vol. 4, no. 14, pp. 5176–5183, 2016, doi: 10.1039/c5ta10416e.
 [152] J. Qian, F. Sun, and L. Qin, "Hydrothermal synthesis of zeolitic imidazolate

- [152] J. Qian, F. Sun, and L. Qin, "Hydrothermal synthesis of zeolitic imidazolate framework-67 (ZIF-67) nanocrystals," *Mater. Lett.*, vol. 82, no. 2012, pp. 220–223, 2012, doi: 10.1016/j.matlet.2012.05.077.
- [153] Y. Ban, Y. Li, X. Liu, Y. Peng, and W. Yang, "Solvothermal synthesis of mixed-ligand metal-organic framework ZIF-78 with controllable size and morphology,"
 Microporous Mesoporous Mater., vol. 173, pp. 29–36, 2013, doi: 10.1016/j.micromeso.2013.01.031.
- 41 [154] Z. Lai, "Development of ZIF-8 membranes: opportunities and challenges for commercial applications," *Curr. Opin. Chem. Eng.*, vol. 20, pp. 78–85, 2018, doi: 10.1016/j.coche.2018.03.002.
- [155] D. Sheberla *et al.*, "High Electrical Conductivity in Ni3(2,3,6,7,10,11-hexaiminotriphenylene)2, a Semiconducting Metal–Organic Graphene Analogue," *J. Am. Chem. Soc.*, vol. 136, no. 25, pp. 8859–8862, Jun. 2014, doi: 10.1021/ja502765n.
- [156] M. G. Campbell, D. Sheberla, S. F. Liu, T. M. Swager, and M. Dincă,
 "Cu₃(hexaiminotriphenylene)₂: an electrically conductive 2D metal-organic
 framework for chemiresistive sensing.," *Angew. Chem. Int. Ed. Engl.*, vol. 54, no. 14,
 pp. 4349–4352, Mar. 2015, doi: 10.1002/anie.201411854.

- 1 [157] H. S. Wang, "Metal-organic frameworks for biosensing and bioimaging applications," 2 Coord. Chem. Rev., vol. 349, pp. 139–155, 2017, doi: 10.1016/j.ccr.2017.08.015.
- 3 [158] C. Dey, T. Kundu, and R. Banerjee, "Reversible phase transformation in proton conducting Strandberg-type POM based metal organic material," *Chem. Commun.*, vol. 48, no. 2, pp. 266–268, 2012, doi: 10.1039/c1cc15162b.
- 6 [159] A. M. Shultz, O. K. Farha, J. T. Hupp, and S. T. Nguyen, "A catalytically active, permanently microporous MOF with metalloporphyrin struts," *J. Am. Chem. Soc.*, vol. 131, no. 12, pp. 4204–4205, 2009, doi: 10.1021/ja900203f.
- 9 [160] S. L. Li and Q. Xu, "Metal-organic frameworks as platforms for clean energy," *Energy Environ. Sci.*, vol. 6, no. 6, pp. 1656–1683, 2013, doi: 10.1039/c3ee40507a.
- 11 [161] Z. Ni and R. I. Masel, "Rapid production of metal-organic frameworks via microwave-12 assisted solvothermal synthesis," *J. Am. Chem. Soc.*, vol. 128, no. 38, pp. 12394– 13 12395, 2006, doi: 10.1021/ja0635231.
- 14 [162] E. Haque, N. A. Khan, H. J. Park, and S. H. Jhung, "Synthesis of a metal-organic framework material, iron terephthalate, by ultrasound, microwave, and conventional electric heating: A kinetic study," *Chem. A Eur. J.*, vol. 16, no. 3, pp. 1046–1052, 2010, doi: 10.1002/chem.200902382.
- 18 [163] H. Jiang, C. Li, T. Sun, and J. Ma, "High-performance supercapacitor material based on Ni(OH)2 nanowire-MnO2 nanoflakes core-shell nanostructures," *Chem. Commun.*, vol. 48, no. 20, pp. 2606–2608, 2012, doi: 10.1039/c2cc18079k.
- [164] C. Zhao, X. Wang, S. Wang, H. Wang, Y. Yang, and W. Zheng, "Pseudocapacitive properties of cobalt hydroxide electrodeposited on Ni-foam-supported carbon nanomaterial," *Mater. Res. Bull.*, vol. 48, no. 9, pp. 3189–3195, 2013, doi: 10.1016/j.materresbull.2013.04.089.
- [165] D. P. Dubal, S. H. Lee, and W. B. Kim, "Sponge-like β-Ni(OH) 2 nanoparticles:
 Synthesis, characterization and electrochemical properties," *J. Mater. Sci.*, vol. 47, no.
 8, pp. 3817–3821, 2012, doi: 10.1007/s10853-011-6236-7.
- 28 [166] P. J. Hall *et al.*, "Energy storage in electrochemical capacitors: Designing functional materials to improve performance," *Energy Environ. Sci.*, vol. 3, no. 9, pp. 1238–1251, 2010, doi: 10.1039/c0ee00004c.
- 31 [167] S. Li, K. Yang, C. Tan, X. Huang, W. Huang, and H. Zhang, "Preparation and applications of novel composites composed of metal-organic frameworks and two-dimensional materials," *Chem. Commun.*, vol. 52, no. 8, pp. 1555–1562, 2016, doi: 10.1039/c5cc09127f.
- [168] J. K. Sun and Q. Xu, "Functional materials derived from open framework
 templates/precursors: Synthesis and applications," *Energy Environ. Sci.*, vol. 7, no. 7,
 pp. 2071–2100, 2014, doi: 10.1039/c4ee00517a.
- 38 [169] G. Jiang, S. Osman, R. A. Senthil, Y. Sun, X. Tan, and J. Pan, "Hierarchically porous carbon derived from magnesium-based metal-organic frameworks as advanced active material for supercapacitor," *J. Energy Storage*, vol. 49, no. January, p. 104071, 2022, doi: 10.1016/j.est.2022.104071.
- [170] R. A. Senthil, S. Osman, J. Pan, X. Liu, and Y. Wu, "Recent progress on porous carbon derived from Zn and Al based metal-organic frameworks as advanced materials for supercapacitor applications," *J. Energy Storage*, vol. 44, no. PA, p. 103263, 2021, doi: 10.1016/j.est.2021.103263.
- In [171] S. Osman, R. A. Senthil, J. Pan, L. Chai, Y. Sun, and Y. Wu, "Hierarchically activated porous carbon derived from zinc-based fluorine containing metal-organic framework as extremely high specific capacitance and rate performance electrode material for advanced supercapacitors," *J. Colloid Interface Sci.*, vol. 591, pp. 9–19, 2021, doi:

50 10.1016/j.jcis.2021.01.109.

- 1 [172] S. Osman, R. A. Senthil, J. Pan, and Y. Sun, "A novel coral structured porous-like amorphous carbon derived from zinc-based fluorinated metal-organic framework as superior cathode material for high performance supercapacitors," *J. Power Sources*, vol. 414, no. December 2018, pp. 401–411, 2019, doi: 10.1016/j.jpowsour.2019.01.026.
- [173] R. A. Senthil, V. Yang, J. Pan, and Y. Sun, "A green and economical approach to derive biomass porous carbon from freely available feather finger grass flower for advanced symmetric supercapacitors," *J. Energy Storage*, vol. 35, no. October 2020, p. 102287, 2021, doi: 10.1016/j.est.2021.102287.
- 10 [174] M. G. Radhika *et al.*, "Electrochemical studies on Ni, Co & Ni/Co-MOFs for high-11 performance hybrid supercapacitors," *Mater. Res. Express*, vol. 7, no. 5, 2020, doi: 12 10.1088/2053-1591/ab8d5d.
- 13 [175] H. Chen *et al.*, "MOF-assisted construction of a Co9S8@Ni3S2/ZnS microplate array with ultrahigh areal specific capacity for advanced supercapattery," *Dalt. Trans.*, vol. 49, no. 30, pp. 10535–10544, 2020, doi: 10.1039/d0dt02127j.
- [176] J. J. Zhou *et al.*, "Boosting Specific Capacity for Supercapattery by in Situ Formation of Amorphous Ni-Co-Borate on MOF-Derived Ni-Co-LDH Nanosheet Array," *ACS Appl. Energy Mater.*, vol. 3, no. 12, pp. 12046–12053, 2020, doi: 10.1021/acsaem.0c02181.
- 20 [177] H. Wu and J. He, "Self-assembled MOF derived Co@C/rGO as positive electrode material for a supercapattery with high energy density," *Diam. Relat. Mater.*, vol. 123, no. February, p. 108912, 2022, doi: 10.1016/j.diamond.2022.108912.
- [178] G. Nagaraju, S. C. Sekhar, B. Ramulu, S. K. Hussain, D. Narsimulu, and J. S. Yu,
 "Ternary MOF-Based Redox Active Sites Enabled 3D-on-2D Nanoarchitectured
 Battery-Type Electrodes for High-Energy-Density Supercapatteries," *Nano-Micro Lett.*, vol. 13, no. 1, pp. 1–18, 2021, doi: 10.1007/s40820-020-00528-9.
- [179] K. Karuppasamy *et al.*, "Unveiling the Redox Electrochemistry of MOF-Derived fcc-NiCo@GC Polyhedron as an Advanced Electrode Material for Boosting Specific Energy of the Supercapattery," *Small*, vol. 18, no. 14, pp. 1–13, 2022, doi: 10.1002/smll.202107284.
- 31 [180] Y. Yan, P. Gu, S. Zheng, M. Zheng, H. Pang, and H. Xue, "Facile synthesis of an accordion-like Ni-MOF superstructure for high-performance flexible supercapacitors," 33 J. Mater. Chem. A, vol. 4, no. 48, pp. 19078–19085, 2016, doi: 10.1039/c6ta08331e.
- [181] S. Anantharaj, K. Karthick, and S. Kundu, "Evolution of layered double hydroxides
 (LDH) as high performance water oxidation electrocatalysts: A review with insights on structure, activity and mechanism," *Mater. Today Energy*, vol. 6, pp. 1–26, 2017, doi: 10.1016/j.mtener.2017.07.016.
- [182] R. Kumari, V. Singh, and C. Ravi, "Enhanced performance of activated carbon-based supercapacitor derived from waste soybean oil with coffee ground additives," *Mater. Chem. Phys.*, vol. 305, no. February, p. 127882, 2023, doi: 10.1016/j.matchemphys.2023.127882.
- 42 [183] J. Gu *et al.*, "MOF-derived Ni-doped CoP@C grown on CNTs for high-performance supercapacitors," *Chem. Eng. J.*, vol. 385, no. November, p. 123454, 2020, doi: 10.1016/j.cej.2019.123454.
- 45 [184] K. Jayaramulu *et al.*, "Covalent Graphene-MOF Hybrids for High-Performance 46 Asymmetric Supercapacitors," *Adv. Mater.*, vol. 33, no. 4, 2021, doi: 47 10.1002/adma.202004560.
- [185] S. N. Ansari, M. Saraf, A. K. Gupta, and S. M. Mobin, "Functionalized Cu-MOF@CNT Hybrid: Synthesis, Crystal Structure and Applicability in Supercapacitors," *Chem. An Asian J.*, vol. 14, no. 20, pp. 3566–3571, 2019, doi:

1 10.1002/asia.201900629.

17

- 2 [186] M. Z. Iqbal, M. M. Faisal, and S. R. A. Meshal Alzaid, "A facile approach to investigate the charge storage mechanism of MOF/PANI based supercapattery devices," *Solid State Ionics*, vol. 354, no. June, p. 115411, 2020, doi: 10.1016/j.ssi.2020.115411.
- 6 [187] Y. Liu, Y. Wang, Y. Chen, C. Wang, and L. Guo, "NiCo-MOF nanosheets wrapping polypyrrole nanotubes for high-performance supercapacitors," *Appl. Surf. Sci.*, vol. 507, no. September 2019, p. 145089, 2020, doi: 10.1016/j.apsusc.2019.145089.
- 9 [188] M. M. Faisal, S. R. Ali, S. K.C., M. W. Iqbal, M. Z. Iqbal, and A. Saeed, "Highly porous terpolymer-MOF composite electrode material for high performance supercapattery devices," *J. Electroanal. Chem.*, vol. 893, no. February, p. 115321, 2021, doi: 10.1016/j.jelechem.2021.115321.
- 13 [189] V. Ramasubbu, F. S. Omar, K. Ramesh, S. Ramesh, and X. S. Shajan, "Three-dimensional hierarchical nanostructured porous TiO2 aerogel/Cobalt based metal-organic framework (MOF) composite as an electrode material for supercapattery," *J. Energy Storage*, vol. 32, no. March, p. 101750, 2020, doi: 10.1016/j.est.2020.101750.